INTERNATIONAL ATOMIC ENERGY AGENCY
UNITED NATIONS EDUCATIONAL, SCIENTIFIC AND CULTURAL ORGANIZATION
INTERNATIONAL CENTRE FOR THEORETICAL PHYSICS
I.C.T.P., P.O. BOX 586, 34100 TRIESTE, ITALY, CABLE: CENTRATOM TRIESTE

H4.SMR/782-25

Second Workshop on
Three-Dimensional Modelling of Seismic Waves
Generation, Propagation and their Inversion

7 - 18 November 1994

Modelling Broad-Band Digital Waveforms
for Moment Tensor Inversion

D. Giardini

III Universita' degli Studi
Istituto Nazionale di Geofisica
Rome, Italy

Three-Dimensional Modelling of Seismic Waves
Generation, Propagation and Their Inversion

Trieste, November 7-18, 1994

MODELLING BROAD-BAND DIGITAL WAVEFORMS FOR MOMENT TENSOR INVERSION

Domenico Giardini
III Università degli Studi, Roma

LECTURE NOTES

Contents:

Preface

Among the outstanding seismological issues is the accurate characterization of complex seismic sources.

The development of digital seismic networks has brought forth a revolution in seismological practice; worldwide seismicity is now routinely analyzed using digital data recorded at global, regional and local scale. Modelling digital waveforms is the main tool of modern seismology for structural and source analyses.

The deployment of global digital seismic networks (GSN, IDA, GEOSCOPE), of regional networks in all continents (MEDNET, CDSN, CNSN, MIDAS, USNSN, ADSN) and of arrays at national or more local scale (for example the networks installed in California by TerraScope, UCSC and UCB) is providing a wealth of high-quality waveforms, (see *Boschi et al., 1991*, for a review of regional and global digital networks).

Moment tensor catalogues have been compiled for more than 11000 events since 1977, chiefly by Harvard University using the CMT method of *Dziewonski et al. (1981)*, replacing traditional earthquake catalogues as the primary tool of seismotectonic analysis. Methods for moment tensor inversion have been proposed using global data (*Dziewonski et al., 1981; Kanamori and Given, 1981; Sipkin, 1986; Romanowicz and Suarez, 1988; Giardini, 1992*) and more recently also regional waveforms (*Holt and Wallace, 1987; Fukushina et al., 1989; Dreger and Helmberger, 1990; Nakanishi et al., 1992; Ritsema and Lay, 1993; Giardini et al., 1993a, 1993b, 1994a, 1994b; Romanowicz et al., 1993; Thio and Kanamori, 1994*); some methods deal specifically with single station inversions (*Ekström et al., 1986; Jimenez et al., 1989; Dufumier and Cara, 1994; Giardini et al., 1994a, 1994b*). Quasi-real time moment tensor inversion is now routinely carried out by several groups for global earthquakes (Harvard, NEIS, Caltech, ERI) and for local and regional earthquakes (Caltech, UCSC, UCB, ING, ERI).

Our goal here is to review and develop methodologies for the characterization of the earthquake source from waveform modelling of digital broadband records. Our target are events of small and moderate size, recorded at local and regional distance. A requisite of many of the methods proposed is the application in real-time and the capability to retrieve a stable source characterization using 3-component records from a single broad-band station, thus providing tools for earthquake monitoring at a single observatory.

The moment tensor is the primary parametrization available to seismologists to provide a first order description of the source that can be derived in consistent manner from single station data. We use a full moment tensor parametrization of the source, which allows to describe and discriminate simple sources with a double-couple mechanism and more complex rupture episodes, characterized by non-planar or multiple faulting. Moment tensors of second or higher order are difficult to retrieve, requiring abundant high-quality data and sofisticated approaches.

By adopting a first-order moment tensor parametrization of the source we implicity assume also a point source model in space and time of the rupture process, thus restricting our analysis to waves with periods always longer than the source duration. For local earthquakes of small dimensions it is still possible to use high-frequency waveforms (around 1 Hz).

A final consideration regards the need to identify and separate the contributions of the source and the propagation effects in the waveforms used for the source analysis. The key element of all approaches is the ability to generate accurate synthetic seismograms to build the inversion kernels; as the synthesis approach is tailored to the frequency and distance range of the waveforms used, it is the characterizing factor of the source analysis.

I: Broad-band seismometry

Ideally a seismogram should resolve the Earth's noise in the whole seismic frequency spectrum, which ranges between a few hertz and a fraction of a millihertz (Figure I.1). In addition, the amplitude of seismic ground motion ranges over many orders of magnitude in the different frequency bands, and the sensor-acquisition system has to cope at the same time with the long period free oscillations of the Earth, with characteristic amplitudes of the order of one micron, and with high-frequency, high-amplitude signal (Figure I.2).

This level of performance was once unattainable, and seismologists were forced to record seismic signal on band-pass instruments. Since 1977 the introduction of digital instrumentation has made possible to reconstruct the broad-band signal from short and long period channels recorded separately – a time consuming, imprecise and delicate task, performed only in limited cases. Nonetheless, the scientific benefits of having access to the whole spectrum of the Earth's displacement have become immediately obvious, and a major effort has been undertaken to make broad-band seismology possible.

A new class of seismometers is now available, characterized by a very wide response spectrum, and the first commercial analog-to-digital converter with 24-bit resolution has been introduced. This, together with improvements in mass storage of data, increased capabilities of microprocessors, higher technology and lower costs in telephone and satellite telemetry, has made possible to design a seismographic station with the required broad-band specifications (*Wielandt and Steim, 1986*).

The new networks consist of isolated seismic stations, controlled by microcomputers which handle the sensors, the digital data stream and the remote communication, performing automatically or on phone request from a distant data centre all the routines once done by a human operator. This allows the installation of very remote stations, of the highest technical standards, far away from marine and anthropic sources of noise to enhance the signal-to-noise ratio of the recorded signal.

The VBB configuration provides flat velocity response in the frequency band from 0.003 Hz to a few Hz, with a full dynamic range of more than 140 dB, encompassing the traditional Short Period and Long Period instruments (Figure I.3). This system is capable of recording on scale ground acceleration over 9 orders of magnitude, from a few nanogals at 300 sec period to nearly 0.1 g at 10 Hz.

A block diagram of a generic VBB station is shown in Figure I.4. The sensor is a 3-component broad-band sensor, capable of providing flat velocity response in the seismic period range up to a few hundred seconds period (commonly the STS-1/VBB force-balanced leaf-spring sensor; *Wielandt and Streckeisen, 1982*). The mass position is always kept close to its center by an electrically generated restoring force; in this way, linearity and stability are requirements of the electronic circuitry rather than of the mechanical assembly. The feedback circuit is modified to expand the response at the low-frequency end.

The analog to digital conversion is performed by a 24-bit ADC for each component, at a usual sampling rate of 20-80 samples per second. The processed seismic signal is characterized by a large dynamic range (140 dB) and excellent linearity, permitting to restore low-amplitude data superimposed on high-amplitude signals without affecting the sensitivity. This for instance allows the extraction of free oscillations even when the high-frequency, high-amplitude signal from a local earthquake is present. A broad-band system can record magnitude-3 events at a few kilometers epicentral distance at less than 1 percent of full scale, without disturbing the simultaneous recording of very-long period signals, and is able to record a magnitude 6 event on scale at about 50 km distance.

To fulfill the potential capabilities of the VBB technology, sites are selected considering the low background noise as the first requirement, at the cost of larger logistical difficulties. Remote sites, away from marine and anthropic sources of noise, are preferred to enhance the signal-to-noise ratio of the recorded signal; they are generally located in underground tunnels, either abandoned mines or specifically excavated, in order to shield the sensors from atmospheric effects like variations in pressure and temperature. A constant monitoring of data quality and noise level is necessary to take full advantage of the high performance of the seismograph. A typical setting for the installation of VBB sensor includes magnetic and electric shields, a vacuum bell cemented to the bedrock and a thermal shield filled with styrofoam. A good coupling between the sensor and the ground rock is essential, as it is the choice of dry, rigid rock.

The availability of VBB technology offers unmatched possilibities for data handling and waveform analysis (Figure I.5) and in recent years numerous waveform modelling methods have been proposed, allowing the characterization of the seismic source across the whole frequency band (Figure I.6).

II: Waveform modelling for moment tensor inversion

II.1: Parametrizing the seismic source

The earthquake rupture process has been traditionally parametrized by magnitude and fault plane mechanism, under the implicit assumptions: (a) faulting takes place on a planar surface and (b) a single parameter can describe the spectral signature of the source. Both assumptions have been known to be crude representations of the reality, but no other approach was allowed by the use of analog data.

More recently, the availability of digital data has introduced more rigor in the source parametrization; even when a point source approximation is introduced it is possible too select the data (wavelength longer than source dimension and wave period longer than source duration) so that the point source condition is truly verified.

The moment tensor is the primary parametrization used by seismologists to provide a first order description of the source. Retrieving the complete moment tensor allows to describe and discriminate seismic sources with a double-couple mechanism and more complex rupture episodes, characterized by non-planar, volumetric or multiple faulting. In particular, a pure double-couple source has no volumetric (isotropic) components, either implosive or explosive, and is thus described by a deviatoric moment tensor with null trace (the sum of the diagonal elements equals zero) and with two eigenvalues of equal value and opposite sign and one null eigenvalue.

The existence of natural earthquakes – that is not due to nuclear explosions, blasts, landslides or slumpings – displaying significant isotropic component or deviation from the double couple has been the subject of heated debate for long time.

The presence of isotropic components has been hotly debated with particular regard to the possibility that phase transitions would play a role in the source generation, mostly in deep focus earthquakes. The predominance of the deviatoric portion of the process has been long demonstrated (e.g. *Honda, 1934; Giardini, 1984*) although the possible presence of a minor volumetric component (not exceeding a few percent) cannot be ruled out (e.g. *Stimpson and Pearce, 1987; Kawakatsu, 1991; Kikuchi and Kanamori, 1994*). In addition, the possible presence of volumetric component has been invoked for

shallow events of small dimensions taking place in volcanic or hydro-thermal areas; as the physical mechanism involved is unclear and the reliability of the results is limited by the noise level of the data, it is difficult to place much significance on the role of volumetric components in crustal earthquakes.

Some earthquakes have been shown to have a source process described by a compensated linear vector dipole (CLVD) (*Giardini, 1983, 1984; Julian and Sipkin, 1985; Kuge and Kawakatsu, 1990, 1992, 1993; Foulger and Julian, 1993*). The CLVD is a deviatoric (nonisotropic) source first described by *Knopoff and Randall (1970)* which corresponds to motion inward towards the earthquake focus along a polar axis (the P Axis), with compensating outward motion symmetrically along the associated perpendicular equatorial plane, or, alternatively, outward motion along the polar axis (the T axis) with compensating inward motion along the equatorial plane. Such a source cannot come about solely due to motion along a fault with simple geometry, e.g. a plane (*Frohlich et al., 1989; Frohlich, 1990*). Although various exotic mechanisms have been proposed to explain the reported CLVD components of earthquake sources (e.g. pure crack opening compensated by fluid injection in volcanic areas), the two most plausible are that most sources consist of two or more suitably oriented double-couple subevents (Figures II.1, II.2) or that many are artifacts caused by systematic errors in the source determination process.

II.2: Strategies for moment tensor inversion

The prime factor in ensuring the capability of extracting reliable source parameters is the ability to model the wave propagation, and thus to separate the contribution of source and propagation in the seismograms. Waveform modelling must be adapted to the period range and epicentral distance of interest, and different strategies for the synthesis of seismograms must be employed.

Three basic approaches can be proficiently used to model seismograms recorded at regional and local distances to invert for the moment tensor:

- VERY LONG-PERIOD MOMENT TENSOR INVERSION: 500-100 SECONDS.
  Seismograms at periods longer than 100 seconds are dominated by surface waves, for shallow earthquakes; accurate complete seismograms can be synthetized by normal mode summation using a global reference model (PREM); the point-source approximation describes all earthquakes (Section II.2.1).
- LONG-PERIOD MOMENT TENSOR INVERSION: 100-30 SECONDS.
  The dispersion of surface waves depends strongly on the lithospheric structure and requires the calibration of phase velocity curves along each path, or of phase velocity maps for whole regions, while amplitudes are not significantly affected; an accurate three-dimensional structural model capable to reproduce all path heterogeneities in the Mediterranean region over the wide frequency band of interest is not available; body waves are a significant component of the seismogram, especially the S phase and its reflections, and can be independently modelled using an average velocity structure if the epicentral distance and the period range allow visual separation from surface waves (Section II.2.2).
- BROAD-BAND MOMENT TENSOR INVERSION: 30-0.5 SECONDS.
  The amplitude of fundamental surface waves down to 5 seconds periods is influenced by the focussing-defocussing effects caused by the laterally heterogeous velocity structure and by lateral variations in Q; surface wave modelling requires sophisticated algorithms dealing with 2-D and 3-D structures; the synthesis of body waves also requires the knowledge of the structural model, but it can be accomplished using depth-dependent velocity models, provided the path is not crossing a steeply dipping interface (subduction areas) or a major structural interface (plate boundaries) (Section II.2.3).

In the following chapters we details the strategy for moment tensor inversions in the different period ranges; applications of these techniques are given in Chapters III-V.

II.2.1: Long-period Moment Tensor Inversion: 500-100 seconds

Our first approach is to constrain the analysis to the very long-period (500-100 seconds) portion of the low-noise spectral window. Indeed, body- and surface-waves at periods exceeding 100 seconds are insensitive to regional-scale heterogeneities in seismic velocity and can be modelled using an average structural model. Further advantages of long-period modelling are the simplicity of the parametrization of the seismic source, taken as a point source, and the availability of efficient codes for the generation of accurate synthetic seismograms, valid also in the near field, by normal modes summation (*Woodhouse, 1988*) using radially symmetric Earth models (PREM; *Dziewonski and Anderson, 1981*).

Our procedure (*Giardini, 1992; Giardini et al., 1993a; 1993b*) computes a centroid-moment tensor solution following these main elements:

- we invert waveforms in the time domain, band-passed in the 8-10 mHz frequency band; for smaller events we choose data windows characterized by higher signal-to-noise ratio; we invert three-components, 20-minutes records, containing long-period body waves and the first orbit of Rayleigh and Love waves;
- a library of complete synthetic seismograms is built, computed at fixed epicentral distances for selected hypocentral depths, by summation of normal modes (*Woodhouse, 1988*) using the PREM model (*Dziewonski and Anderson, 1981*);
- a time shift is computed for each trace, accounting for the source half-duration, for the centroid mislocation of large earthquakes and for any phase contamination due to a strongly heterogeneous path;
- we select narrow, nearly monochromatic frequency ranges (usually 5-7 mHz or 8-10 mHz), a procedure which warrants the use of single frequency-independent correction terms; multiple inversions are carried out in neighboring narrow frequency ranges;
- we perform single and multiple station inversions;
- the source process is parametrized with the full moment tensor and the added constraint of null volumetric component, while we do not impose a pure double-couple solution;
- depth is constrained by variance minimization on inversions at different trial depths, following *Romanowicz and Suarez (1983)*;
- we perform several tests to assess the stability of the moment tensor solution, both in terms of seismic moment and source geometry; among these, we apply a minimization scheme to reduce the variability associated to the $M_{r\theta}$ and $M_{r\varphi}$ components of the moment tensor.

Applications are in Chapter III.

II.2.2: Long-period Moment Tensor Inversion: 100-30 seconds

A second approach (*Giardini et al., 1994a, 1994b*) focuses on the inversion of surface waves adopting a regionalized, frequency dependent phase-velocity model to account for the 3-D litospheric structure. This method cannot be extended to higher frequencies,

as the focussing and defocussing due to lateral heterogeneities in velocity and the laterally varying Q induce large amplitude effects on surface waves, requiring 2-D and 3-D modelling. This approach is based on two considerations: (a) a global average model (ex. PREM) can reproduce quite accurately the amplitude of surface waves down to periods of 30-40 seconds, and (b) what is required is thus a simple strategy to calibrate the phase velocity along each path in the 40-100 seconds period range.

Modelling complete long-period regional waveforms (in the 100-3000 km distance range and 30-100 seconds period range) is a complex exercise, due to theoretical and practical limitations. Body and surface waves overlap in time in the seismogram at close distances, posing serious problems of separation and modelling; body waves can be modelled using a standard stratified model, while surface waves require the accurate calibration of dispersion curves (Figure II.3), which have been calibrated with sufficient accuracy only in very few locations around the world.

We develop algorithms for moment tensor inversion using complete three-components waveform records and calibrating dispersion curves of phase velocity for fundamental Rayleigh and Love waves; while the dispersion curves can be classically used in a inversion scheme (e.g. a pure-path method) for the determination of the velocity structure, we are interested here in their application in waveform inversions for source analysis and we test two different approaches to the determination of group and phase velocity calibrations. A second goal is to verify the accuracy of single-station moment tensor determinations in narrow-band and wide-band inversions for application in routine monitoring of seismic sequences and regional seismicity.

The analysis of earthquakes of moderate size (M_W=4-6) requires the modelling of body and surface waveforms in the 10-30 mHz frequency range. Body waves can be modelled in amplitude and phase in the 10-30 mHz band using a standard stratified model; the amplitude of surface waves can be reproduced by an average structural model, while phase modelling requires the use of accurate dispersion curves. For example, lithospheric models for large parts of the European-Mediterranean region have been published (e.g. *Panza et al., 1980; Calcagnile et al., 1982; Snieder, 1988; Nesterof and Ianovskaia, 1988; Dost, 1990*); however, an accurate 3-D structural model accounting for the structural complexity of the whole area, especially south of the seismic belt, valid over the wide period range of interest, is not available.

Forward modelling demonstrates that a moment tensor solution obtained at low frequency (5-7 mHz) can reproduce the amplitude spectra in the wide frequency range 8-26 mHz. significant amplitude discrepancies are observed. If the phase of the synthetic

spectra is corrected with smoothed phase shifts derived from the data spectra, the fit between data and synthetics in time domain is good across the frequency band of interest.

To model the complete waveforms of the mainshock and of the smaller aftershocks in the 10-30 mHz frequency band we derive group and phase velocity dispersion curves from records of significant earthquakes using two different approaches:

1: CALIBRATION OF PHASE VELOCITY DISPERSION

With reliable source mechanism and duration available from low-frequency (5-7 mHz) moment tensor inversion, we derive the phase velocity for fundamental surface waves along each path, by smoothing the phase difference between the spectra of data and synthetics across the frequency band of interest. Locating the long-period space-time centroid of the source is essential for large earthquake, to avoid contaminating the phase velocity calibration (cfr. *Nakanishi and Kanamori, 1982*). In a single station scheme, a normalization must be introduced; we set the phase velocity at 10 mHz to coincide with that predicted by a global standard model like PREM, a condition largely verified in practice at regional distances (*Kulhanek, 1990*) and in global tomographic inversions (*Ekström, 1994*; personal comunication).

We derive separate phase corrections from the radial, vertical and transversal components to obtain smoothed dispersion curves of Rayleigh and Love fundamental modes. To test for the stability of the phase corrections, we derive the calibrations for different events in the same sequence and apply them to smaller events.

2: MFT CALIBRATION OF GROUP VELOCITY DISPERSION

The Multiple Filter Technique (MFT) was first introduced for the determination of group velocities of dispersed signals (*Dziewonski et al., 1969; Dziewonski and Hales, 1972*). The MFT has been extensively used, for example to estimate modal spectral amplitudes (*Herrmann, 1973*), for source studies (*Mills and Fitch, 1977; Herrmann et al., 1981*), for determination of Q structure (*Cheng and Mitchell, 1981*) and to measure the ellipticity of Rayleigh waves (*Saxton et al., 1977*). *Herrmann (1987)* implemented the MFT in his program package for surface waves analysis. Details on the MFT are given in Appendix A.

The main elements of this approach are:

- to use the initial reference library of synthetic seismograms computed at fixed epicentral distances for selected hypocentral depths for the 1-D model (PREM);

- to compute phase correction curves for Rayleigh and Love waves in the 40-100 seconds band by smoothing phase differences between data and synthetics on specific station-event paths for moderate-large earthquakes, using moment tensor solutions derived at low frequency;
- to build a library of phase correction curves for calibrated paths;
- to invert for the moment tensor in multiple frequency bands by combining the libraries of synthetic seismograms and of phase correction curves, following the approach outlined above.

As we need phase calibration for the waveform inversion, we derive phase velocity dispersion curves from the group velocity curves by requiring that the phase velocity be equal to the PREM at 10 mHz, a condition largely verified in practice (*Kulhanek, 1990*; personal comunication, *Ekström, 1994*).

The propagation of surface waves along a major arc is assumed in our approach; focussing and defocussing of surface wave paths due to lateral heterogeneities in velocity and Q can produce large amplitude effects at higher frequency, requiring 2-D and 3-D modelling (e.g. *Snieder, 1988*). These effects, however, are negligible at regional distances and in the frequency range considered.

Applications are in Chapter IV.

II.2.3: Broad-band Moment Tensor Inversion: 30-0.5 seconds

Recently some experiments with broadband regional data (*Dreger and Helmberger, 1990; Zielhuis and Nolet, 1991*) have shown that the use of stratified models allows to reproduce the main characteristics of seismograms at local and regional distance, for relatively simple tectonic environments. Here we verify the limits of application of stratified models for source analyses at regional scale.

Several considerations can be made. The use of stratified model to fit regional waveforms implies averaging the heterogeneities along the source-station path; this approximation adapts better to surface waves, which for their nature sample with a low frequency spectral content all the shallow structure along the source-station path. Body waves instead are sensitive to the superficial structure near the source and the station, while travelling mostly at depth along the rest of the path. It is thus likely that, especially at high frequency, a model representing a good average structure for surface

waves will not reproduce adequately the body waves; a typical example is the case of hypocenter and station located on continental margins and the path crossing through an oceanic basin.

A second consideration regards the need to make use of body and surface surface waves on a wide band of frequencies. Indeed, the problem of obtaining a structural model from monochromatic surface waves is highly non-univocal; the use of surface waves spanning a large frequency range adds structural resolution with depth, while modelling body waves allows to constrain the hypocentral depth, the impedance layering near the surface, the depth of the main deep interfaces, and a mean deep structure.

The investigation of the lithospheric structure through inversion techniques has been attempted, although these methods are applicable only in the case of very simple structural models (at most one layer over a halfspace) and generally for small epicentral distance; they are not applicable to model a complete seismogram at regional distance in the case of a multi-layered structural model.

Usually we employ a trial-and-error procedure, constraining the initial model with known structural elements along the path and adjusting the model to reproduce the observed characteristics of the signal: the relative amplitude of the surface and body waves, the complexity of the body waves, the duration of the surface waves coda, the arrival times of the P, S and surface waves phases. Once a good average model is found, we reproduce separately the fine structure of body waves phases at higher frequencies to calibrate the depth and impedance of the main interfaces, remaining close to the mean model.

Since we use a point source representation of the source we position our analysis in the flat portion of the displacement source spectrum. The high-frequency limit of our analysis is thus connected to the source duration; for a moderate earthquake (e.g. the Eastern Sicily event of December 13, 1992, with $M_0 = 3.7 \times 10^{24} dyne \cdot cm$), the expected duration of the fault is of few seconds and we model waves in the 5-50 period range. In the case of a smaller event we can use waves to 1 second period.

Complete synthetic seismograms can be computed efficiently for a layered structure following the modal or the reflectivity approach. The reflectivity method has been widely used in the literature (*Fuchs and Muller, 1971; Kennett, 1983*). Here (Appendix B) we develop an algorithm to model body waves ($P - SV$, SH) and surface waves, based on the full reflectivity approach, following the formulation of *Woodhouse (1980)*.

While reflectivity algorithms are now readily available, we preferred to conduct our

own development, as these codes require extensive testing; for example, for the definition of the step and range for the integration in frequency and wave number. Comparative tests against published algorithms allowed the verification of the numerical accuracy of our procedure; a significant difference emerged in the comparison with published synthetics and was confirmed by the author to be due to errors on his side (*Kennett, personal comunication*).

The advantages of adopting an analytic solution lie in the rapidity of calculus, in the accuracy and completeness of the synthetics, in the explicit integration over the plane ω–k, making possible the a priori choice of the frequencies and the branch to model. The use of depth-dependent velocity distributions limits the modelling to relatively simple structural environments. Dispersion and attenuation are introduced by choosing elastic parameters with an imaginary component (*Woodhouse, 1980; Kennett 1983*).

III: Applications of very long-period moment tensor inversion

We present applications of the methodology described in Section II.2.1 for very long-period moment tensor inversion (500-100 seconds) for global, regional and local earthquakes and the results of specific experiments designed to test the accuracy and reliability of the moment tensor solutions.

III.1 Large global earthquakes of 1990

1990 was characterized by a series of large earthquakes distributed worldwide: March 3 (Fiji) and 25 (Costa Rica), May 12 (Sakhalin), 20 (Sudan) and 30 (Romania), June 20 (Iran), July 16 (Luzon) and December 30 (New Britain).

For all these events, the NEIC Monthly Bulletins report m_b values, fault plane solutions derived from polarities, Harvard CMTs and, for some of them, a long-period moment tensor solution by USGS. Here we compute moment tensor solutions using digital wavforms collected by the MEDNET network. Table III.1 lists earthquake parameters used and obtained in this study: hypocentral locations from the CMTs (depths for the deep events are computed here), m_b, and seismic moments M_0 obtained in this study (in dyne·cm). Figure III.1 displays the fault plane solutions on a world map; we use the best double-couple definition of *Dziewonski et al. (1981)*. The events span the epicentral distance range between 10° and 160°; three events are deep: May 12 (Sakhalin, 590 km), May 30 (Romania, 85 km) and December 30 (New Britain, 200 km).

Figure III.2 compares the fault plane solutions and seismic moments obtained here with the CMTs, the moment tensors by USGS and the fault plane solutions by NEIC. Our solutions are very stable and compare well with the CMTs, both in geometry and in size, whereas more pronounced discrepancies exist between the MEDNET and CMTs solutions and the moment tensors by USGS; of the five events analyzed with this method by USGS and reported by NEIC, the seismic moment of the March 3 event is much smaller and a different geometry is shown for the December 30 event. Discrepancies in source geometry are observed also with respect to the NEIC fault plane solutions for

the March 25 and December 30 events.

Figure III.3 displays examples of waveform modelling: station VSL for the May 12, Sakhalin event and station MDT for the June 20, Iran event. We obtain a good fit between data and synthetics for the dominant, sharp surface-waves packages as well as for the body-wave trains. We note that, although these solutions are obtained using 200-130 seconds waves, the correspondence between data and synthetics extends to much longer periods for these large events, up to 500-1000 seconds; horizontal components are generally more noisy than vertical ones. Slight phase discrepancies can be sometimes observed for later-orbits surface-waves trains; this small effect, induced by the mantle heterogeneity, is only partially corrected by our use of a single time term for each trace and could be further reduced by introducing a three-dimensional mantle model in the synthesis of the kernels (*Woodhouse and Dziewonski, 1984*).

III.2 Significant earthquakes of the Mediterranean: 1990-1992

In 1990-1992 the Mediterranean was hit by disastrous earthquakes on June 20, 1990 in Iran (55.000 casualties), March 13, 1992 in Turkey (1.500 casualties) and October 12, 1992 in Egypt (550 casualties). We derive moment tensor solutions for 20 events covering the area between Iran and the Azores; we compute the moment tensor using the algorithm outlined above and the hypocentral location and origin time broadcasted by ING and NEIC, and we compare source geometry and seismic moment with those derived by the CMT method. Table III.2 lists significant earthquake parameters: hypocentral locations and magnitudes m_b from NEIC and ING and seismic moments M_0 obtained here (in $dyne \cdot cm$).

Figure III.4 displays the fault plane solutions on a regional map (we use the best double-couple definition of *Dziewonski et al., 1981*). In Figure III.5 we compare source geometries and seismic moments obtained here and with the CMT method; the comparison is positive both in geometry and in size. Significant geometry differences are observed only for three events of small dimensions (n.1,6,11), for which only a few vertical records were available for our analysis, since the Earth is consistently noisier on horizontal components. We note, however, that for these three small events the CMT geometry produces significantly higher misfit and is thus incompatible with the MEDNET data. We do not find any event with stable, high deviation from the double couple mechanism. Figure III.6 displays examples of waveform modelling.

III.3 Single station inversion

A question we would like to answer is the feasibility of obtaining moment tensor solutions from single station records, to activate real-time procedures of seismic monitoring using a single VBB observatory. We show a test conducted for the December 13, 1990, Eastern Sicily, earthquake. In the immediate aftermath of the event the only available size estimates were a preliminary $M_D = 4.9$ (ING) and a reported maximum intensity I=VII-VIII; since the rapid determination procedures of EMSC and NEIC were not triggered, further magnitude estimates were provided only much later, with values ranging between 5.1 and 5.9. In addition, consistent estimates of the focal geometry were derived only later using arrivals from teleseismic stations (*Amato et al., 1991; De Rubeis et al., 1991*) and by waveform modelling (CMT).

Figure III.7 shows the focal mechanisms obtained by inverting the joint MEDNET data and in single station inversions; for comparison also the CMT mechanism and two fault plane solutions (S1, *Amato et al., 1991*; S2, *De Rubeis et al., 1991*) are also displayed. The agreement obtained by inversion of single station data is very encouraging, indicating that even a single VBB station permits reliable control on the seismic source of regional earthquakes (as shown for teleseismic events in *Ekström et al., 1986*). The seismic moment $M_0 = 3.7 \times 10^{24} dyne \cdot cm$ corresponds to magnitude values of $m_b = 5.5$, $M_S = 5.7$, $M_W = M_L = 5.8$ (using regression laws from *Heaton et al., 1986*).

More single station inversions will be included in Chapter V.

III.4 Uncertainties in moment tensor assessment

The issue of providing formal errors in moment tensor inversions has long been discussed (see *Dziewonski et al., 1981*), since standard errors are known to underestimate true uncertainties. A partial estimate of the uncertainty on the seismic moment for a well constrained moment tensor solution (the November 23, 1980, Irpinia earthquake; *Giardini, 1993*) may be estimated from a misfit curve (Figura III.8), showing an error of about $\pm 0.2 dyne \cdot cm$, corresponding approximately to a ± 0.1 uncertainty in m_b.

In addition, we may estimate the uncertainty associated with the single independent elements of the moment tensor; as it is common for shallow events, we observe a larger

instability associated with the the $M_{r\theta}$ and $M_{r\phi}$ components of the moment tensor, which we reduce applying a weak minimization scheme in the inversion, as shown by a test for the May 20, 1990, Sudan earthquakes (Figure III.9). A non-constrained solution (MT1) has a large seismic moment of $8.2 \times 10^{26} dyne \cdot cm$, dominated by the $M_{r\theta}$ and $M_{r\phi}$ components, and reaches a good variance of R=.213. By increasing the constraint, the $M_{r\theta}$ and $M_{r\phi}$ components decrease significantly, and so does the seismic moment, while the other moment elements remain unchanged and the variance increases only slightly. It is only with a very strong contraint (ϵ=1.0) that the solution (MT5) degrades considerably (R=.449), and all moment tensor elements are reduced ($M_0 = 2. \times 10^{26} dyne \cdot cm$). The geometry of the focal mechanism reflects the proportions of the moment tensor elements (Figure III.9b); unconstrained solutions are dominated by the dip-slip elements $M_{r\theta}$ and $M_{r\phi}$, whereas more constrained tensors show a strike-slip geometry. The final solution MT3 is chosen on the basis of the resolution of the inversion procedure, and shows a superposition of dip-slip and strike-slip components.

The same test test for the Eastern Sicily event (Figure III.10) shows that the moment tensor solution is stable unless a very strong constraint on the moment size is applied. Solutions with a wide range of minimization parameters ($\epsilon = 0.0-0.05$) have very similar moment tensor elements; the $M_{r\theta}$ and $M_{r\phi}$ components of the moment tensor are always rather small, as the moment tensor is dominated by the strike-slip $M_{\theta\phi}$ component; the seismic moment for these four inversions decreases from 4.0 to $3.7 \times 10^{24} dyne \cdot cm$, while the normalized variance remains in the 0.043-0.045 range. Only with a very strong constraint ($\epsilon = 1.0$) the solution degrades considerably (variance =.13) and the seismic moment diminishes to $2.5 \times 10^{24} dyne \cdot cm$. As the moment tensor in all cases is dominated by the strike-slip components, its geometry remains stable.

III.5 Depth dependence

The determination of the hypocentral depth is not among our goals, since we do not have sufficient data for this task and we invert waves in an almost mono-chromatic frequency band; we would rather prefer the method to have limited depth resolution and dependence, to ensure good stability of the results, even with wrong initial depth. To this purpose we show in Figure III.11 the moment tensor and the variance obtained in inversion tests at different trial depths for the deep May 12, Sakhalin earthquake. The results are very encouraging; the variance curve constrains the depth within ± 20

km, while the fault geometry remains stable over an extended depth range and the seismic moment varies by 5%.

Figure III.12 shows three different depth depencences for shallow events in the Mediterranean. The 1991 Caucasus earthquake is contrained to a very shallow depth, the 1992 Eastern Sicily to a deeper crustal rupture, while little resolution is shown by the results for the 1990 Iran event.

Figure III.13 shows more details on the depth dependence of the solution for the Eastern Sicily earthquake; we display the normalized variance, the focal mechanism and the seismic moment obtained at different trial depths. The variance curve with depth shows the hypocenter to be rather deep for a crustal earthquake; the acceptable depth range is 15-30 km, with seismic moment ranging between 3.7 and 3.9 $\times 10^{24} dyne \cdot cm$.

Figure III.14 shows the normalized variance and the seismic moment obtained at different trial depths for the NW Iran event of 1990; while the variance is insensitive to the hypocentral depth, the seismic moment increases at depths below 35 km, constraining the hypocentral depth in the first 30 km.

IV: The 1990 NW Iran sequence

To illustrate the reliability of the inversion procedures developed in Section II.2.2 for moment tensor determination in case of complex source, we process complete waveforms in the 100-30 seconds band from a single station at regional distance for the 1990 NW Iran earthquake sequence (the events of June 20, 21 and 24).

The Rudbar-Tarom or Manjil earthquake of June 20, 1990 occurred in the western Alborz mountain belt in northwestern Iran, southwest of the Caspian Sea (*Moinfar and Naderzadeh, 1990; Berberian et al., 1992*). With magnitude $M_S = 7.6$ and moment $M_0 = 1.56 \times 10^{27} dyne \cdot cm$ ($M_W = 7.4$), it was the largest earthquake to hit that area in historical times, killing more than 40.000 people and destroying three cities and 700 villages. Surface faulting and folding were observed in the epicentral area; three main segments of co-seismic surface break were observed, for a total legth of at least 80 km and with maximum left-lateral displacement of 60 cm. Two large aftershocks took place on June 21 ($M_W = 5.7$) and June 24 ($M_W = 5.3$).

Figure IV.1 (modified after *Berberian et al., 1992*) shows a map of the epicentral area of the the 1990 NW-Iran earthquake sequence, the macroseismic fields of intensity larger than MCS=VII, the surface faulting, the location and mechanisms of the June 20 mainshock and the June 21 and 24 aftershocks determined in this study.

To obtain a moment tensor solution for the June 20 mainshock, we invert 6 hours of three-components waveforms recorded by the MEDNET stations of MDT, VSL, AQU and BNI, band-passed in the 5-7 mHz frequency band (waveform modelling for station MDT is shown in Figure III.3).

The seismic moment ($1.1 \times 10^{27} dyne \cdot cm$) and the almost pure strike-slip mechanism with a fault plane striking WNW are in agreement with the CMT solutions obtained by Harvard ($1.35 \times 10^{27} dyne \cdot cm$; *Dziewonski et al., 1991*), NEIS ($1.1 \times 10^{27} dyne \cdot cm$), Caltech ($1.0 \times 10^{27} dyne \cdot cm$; *Thio et al., 1990*) and by *Berberian et al.* (*1992*; $8.8 \times 10^{26} dyne \cdot cm$) [see also *Giardini, 1992*].

Forward modelling (Figure IV.2) shows that the moment tensor solution obtained at low frequency (5-7 mHz) can reproduce the amplitude spectra in the wide frequency range 8-26 mHz for the 1990 mainshock. Only at frequencies approaching the corner frequency of this large event, with a centroid half-duration of 15 seconds (*Dziewonski et al., 1991*), significant amplitude discrepancies are observed. If the phase of the synthetic

spectra is corrected with smoothed phase shifts derived from the data spectra, the fit between data and synthetics in time domain is good across the frequency band of interest.

To model the complete waveforms of the mainshock and of the smaller aftershocks in the 10-30 mHz frequency band we derive group and phase velocity dispersion curves from records of the June 20 mainshock using two different approaches, as explained in Section II.2.2. In Figure IV.3 we show the dispersion diagram for the vertical component of VSL station for the 1990 Iran mainshock obtained using the MFT. The dispersion of the fundamental Raylegh mode is clearly visible; group velocities overlap those predicted by PREM in the 8-17 mHz frequency windows but are significantly lower at higher frequencies.

Figure IV.4 summarizes the results obtained for phase and group velocity dispersion for the VSL recordings of the 1990 Iran mainshock. In Figure IV.4a-b we compare group velocity dispersion curves for fundamental Rayleigh and Love waves from PREM and for typical oceanic and continental paths with those derived using MFT; the observed Rayleigh and Love group velocities follow quite closely the dispersion curve of a typical continental path (the Rayleigh waves group velocities are even lower around 25 mHz frequencies). Indeed, the path followed by the surface waves from the Alborz mountains to the Sardinia Island follows the lower Atlas and the Anatolian plate before crossing a more complex region including the lower Dinarides, the Adriatic microplate, the Apennines and the Tyrrhenian Sea; of these tectonic blocks, only the Tyrrhenian Sea has a clear oceanic structure.

In Figure IV.4c we compare phase velocity dispersion curves for Rayleigh and Love fundamental modes from PREM with those derived using MFT and with the unsmoothed phase delays of the 1990 mainshock. The MFT curves produce an excellent fit to the unsmoothed phase delays of the 1990 mainshock, confirming that the phase velocity derived directly from waveform fitting are not contaminated by body waves arrivals.

Using the phase velocity dispersion curves for Rayleigh and Love fundamental modes shown in Figure IV.4, we adjust the phase of the Rayleigh and Love fundamental modes in our kernels and invert for the moment tensor of the mainshock and aftershocks of the Iran 1990 sequence from the VSL three-component records filtered in narrow and wide frequency bands.

Figure IV.5 display the results for the June 20, June 21 and June 24 events; the seismic moment and the frequency band used are indicated for each solution and the

Harvard CMT solution is shown for comparison.

We obtain very stable results for the June 20 mainshock over the whole 8-30 mHz band; only at frequencies above 26 mHz, as explained before, we do observe minor amplitude contamination due to the large dimensions and long duration of this event. Comparable results are obtained using frequency bands as narrow as 2 mHz. The seismic moment ($M_0 = 1.56 \times 10^{27} dyne \cdot cm$) in the single station inversion is higher than the value obtained using uncalibrated multiple stations (cfr. the Harvard CMT estimate of $1.35 \times 10^{27} dyne \cdot cm$). As the focal geometry we obtain is the same obtained in the multiple-station CMT, this effect is attributed to to the accurate phase and amplitude match achieved in the single station inversion, resulting in misfit ratios better than 0.05 for noise-free records and, barring minor site amplification factors, in a reliable seismic moment estimate. The variation of seismic moment in different inversions (Figure IV.5a) corresponds to $M_W = 7.3 - 7.5$, and is comparable to the spread observed in the multi-stations CMT solutions obtained by other authors.

Similar consistency in narrow-band and wide-band inversions is achieved also for the June 21 (Figure IV.5b) and June 24 (Figure IV.5c) aftershocks. We obtain values of $M_0 = 3.9 \times 10^{24} dyne \cdot cm$ ($M_W = 5.7$) for the June 21 event and $M_0 = 1.0 \times 10^{24} dyne \cdot cm$ ($M_W = 5.3$) for the June 24 event in good agreement with the Harvard CMT solutions.

In Figures IV.5b-c we display the full moment tensor for our solutions and the CMTs. For the June 21 event this is done to show the consistency of our results across the whole 10-30 mHz band and the similarity with the CMT solution. For the June 24 event there is a discrepancy between the Harvard CMT best double couple, a pure strike-slip similar to the mainshock, and our best double couple, a reverse mechanism very similar to that of the June 21 event (Figure IV.1). This discrepancy is only illusional, as both our and the Harvard moment tensors are characterized by consistent deviation from a pure double couple mechanism. The full moment tensor plots of Figure IV.5b-c show the solutions to be in good agreement.

Appendix A: Synthetic seismograms by full reflectivity method

The response of a horizontally stratified medium to a point source is obtained by integration over frequency (ω) and wave number (κ) (*Hudson, 1969*). If the medium is isotropic, the response is conveniently separated in the $P-SV$ and SH components. In a polar cylindrical coordinate system (z,r,φ), a point source at depth $z = z_S$ produces an elastic displacement field:

$$\mathbf{u} = \mathrm{u}(z,r,\varphi) = \int_{-\infty}^{\infty} d\omega e^{i\omega t} \sum_{m=-\infty}^{\infty} \frac{1}{2\pi} \int_0^{\infty} k\, dk \left\{ b_1^S \mathbf{R}_k^m + b_2^S \mathbf{S}_k^m + b_1^T \mathbf{T}_k^m \right\}$$

where $\mathbf{R}_k^m$, $\mathbf{S}_k^m$ and $\mathbf{T}_k^m$ are spherical harmonic functions (*Takeuchi and Saito, 1972*).

The coefficients $b_1^S(z,k,m,\omega)$ and $b_2^S(z,k,m,\omega)$ are elements of the four components stress-displacement vector $\mathbf{b}^S$, linked to the components of motion $P-SV$; similarly, $b_1^T(z,k,m,\omega)$ is an element of the two components stress-displacement vector $\mathbf{b}^T$, linked to the component of motion SH. The two vectors, for k,m and ω fixed, are solution of the system of differential equations

$$\begin{cases} \partial_z \mathbf{b}^S = \omega A^S \mathbf{b}^S & (z_a < z < z_s, z_s < z < z_b) \\ \partial_z \mathbf{b}^T = \omega A^T \mathbf{b}^T & (z_a < z < z_s, z_s < z < z_b) \end{cases} \tag{1}$$

The matrices A^S and A^T are defined for each homogeneous layer of the depth-dependent structural model. Boundary conditions in z_a and z_b will depend on the specific problem; generally, every solution for $\mathbf{b}^S$ will be a linear combination of two elementary vectors which, in the case of free surface in z_a, impose a condition of null traction, or, at the bottom of the structure for z_b, correspond to $P-SV$ waves propagating in the half-space below. The vectors $\mathbf{b}^S$ and $\mathbf{b}^T$ admit only one discontinuity in correspondence of the seismic source

$$[\mathbf{b}^S]_{z_s-0}^{z_s+0} = \mathbf{s}^S \quad [\mathbf{b}^T]_{z_s-0}^{z_s+0} = \mathbf{s}^T$$

where $\mathbf{s}^S$ and $\mathbf{s}^T$ can be written as function of the elements of the tensor moment M(t) (*Hudson, 1969*) and the spectrum of the source is defined as

$$\overline{M}(\omega) = \frac{1}{2\pi} \int_0^{\infty} M(t)\, e^{-i\omega t}\, dt$$

The analytical solution of the differential equation system (1) for the components $P-SV$ is given by the *propagator* $P(z,z_0)$:

$$P(z,z_0) = exp[\omega A^S (z - z_0)]$$

with the initial condition $P(z_0,z_0) = \mathbf{I}$. Physically the propagator describes the stress-displacement vector $\mathbf{b}^S(z)$ in any point of the medium when $\mathbf{b}^S(z_0)$ is known:

$$\mathbf{b}^S(z) = P(z,z_0)\mathbf{b}^S(z_0)$$

A similar solution can be obtained for the SH component. *Woodhouse (1980)* develops the full expansion for the P-SV field; we derive here the SH formulation.

To apply the boundary conditions, $\mathbf{b}^S$ and $\mathbf{b}^T$ are propagated from the source in z_s to the free surface in z_a and to the limit with the halfspace below in z_b, by successive multiplication of the propagators corresponding to the different layers in the structure

$$\mathbf{b}^S(z_a) = P(z_a,z_1)P(z_1,z_2).....P(z_{N-1},z_s)\mathbf{b}^S(z_s)$$

The progressive application of the propagator can lead to loss of numerical precision when modelling high frequency waves in a multi-strata structure; to avoid this problem we follow the scheme proposed by *Gilbert and Backus (1966)* and developed by *Woodhouse (1980)*. For any two solutions of the system, $\mathbf{b}_1^S$ and $\mathbf{b}_2^S$, the vector of the six anti-symmetric products of their elements

$$[b_{1i}^S b_{2j}^S - b_{1j}^S b_{2i}^S]_{i \neq j}$$

defined *minor*, satisfies a sixth-order differential equation system, derived from the system for $\mathbf{b}^S$; the propagation of minors avoids numerical instabilities and loss of precision.

The advantages of adopting an analytic solution lie in the rapidity of calculus, in the accuracy and completeness of the synthetics, in the explicit integration over the plane ω–k, making possible the a priori choice of the frequencies and the branch to model. The use of depth-dependent velocity distributions limits the modelling to relatively simple structural environments. Dispersion and attenuation are introduced by choosing elastic parameters with an imaginary component (*Woodhouse, 1980; Kennett 1983*).

Appendix B: the Multiple-Filter Technique

The Multiple Filter Technique (MFT) was first introduced for the determination of group velocities of dispersed signals (*Dziewonski et al., 1969; Dziewonski and Hales, 1972*). The MFT has been extensively used, for example to estimate modal spectral amplitudes (*Herrmann, 1973*), for source studies (*Mills and Fitch, 1977; Herrmann et al., 1981*), for determination of Q structure (*Cheng and Mitchell, 1981*) and to measure the ellipticity of Rayleigh waves (*Saxton et al., 1977*). *Herrmann (1987)* implemented the MFT in his program package for surface waves analysis.

In the MFT, a gaussian filter $H(\omega)$, defined as:

$$H(\omega) = \begin{cases} e^{(-\alpha(\omega-\omega_0)^2/\omega_c^2)} & \mid \omega - \omega_0 \mid \leq \omega_c \\ 0 & \mid \omega - \omega_0 \mid > \omega_c \end{cases}$$

where $\omega_c = \omega_0(\pi/\alpha)^{\frac{1}{2}}$, is applied to the Fourier transform $A(\omega,r)e^{-j(k(\omega)r-\phi)}$ of a dispersive waveform that propagates at distance r from the source.

The envelope of the filtered time signal has the form:

$$g(t,r) = \frac{A(\omega_0,r)}{2\pi}\omega_0\left(\frac{\pi}{\alpha}\right)e^{(-\omega_0(t-r/U_0)^2/4\alpha)}$$

and will reach its maximum at t^*, travelling with group velocity $U = r/t^*$.

Dziewonski et al. (1972), using MFT on synthetic seismograms, showed that group velocity determination by MFT has systematic errors when the group velocity changes rapidly with frequency; this error can be reduced by increasing α in the equations above, but a large α affects the temporal resolution of interfering modes (*Herrmann, 1973*). The problem of spectral biasing due to frequency domain filtering of surface waves seismograms has been investigated in details by *Russel et al. (1988)*. After some experimentation, we opted for a frequency independent $\alpha = 4\pi$, yielding $\omega_c = \omega_0/2$.

We find that the MFT allows to discriminate efficiently between Love and Rayleigh fundamental modes and improves the capability of discriminating between surface and body wave signals arriving with the same group velocity.

References

AMATO A., AZZARA, R., BASILI, A., CHIARABBA, C., COCCO, M., DI BONA, M. and SELVAGGI, G. (1991): La sequenza sismica del Dicembre 1990 nella Sicilia Orientale: analisi dei dati sismometrici, in E. Boschi and A. Basili (eds.), *Contributi allo studio del terremoto della Sicilia Orientale del 13 Dicembre 1990*, Publication of the Istituto Nazionale di Geofisica 537, 57-84.

BERBERIAN, M., M. QORASHI, J.A. JACKSON, K. PRIESTLEY and T. WALLACE (1992): The Rudbar-Tarom earthquake of 20 june 1990 in NW Persia: preliminary field and seismological observations, and its tectonic significance, *Bull. Seism. Soc. Am.*, **82**, 1726-1755.

BOSCHI, E., D. GIARDINI and A. MORELLI (1991): MedNet: the Broad-Band seismic network for the Mediterranean, *Il Cigno Galileo Galilei*, Roma.

CALCAGNILE, G., F. D'INGEO, P. FARRUGIA and G.F. PANZA (1982): The lithosphere in the Central Eastern Mediterranean Area, *Pure Appl. Geophys.*, **120**, 389-406.

CHENG, C.C. and J. MITCHELL (1981): Crustal Q structure in the United States from multi-mode surface waves, *Bull. Seism. Soc. Am.*, **71**, 161-181.

DE RUBEIS, V., GASPARINI, C., MARAMAI, A. and ANZIDEI, M. (1991): Il terremoto Siciliano del 23 Dicembre 1990, in E. Boschi and A. Basili (eds.), *Contributi allo studio del terremoto della Sicilia Orientale del 13 Dicembre 1990*, Publication of the Istituto Nazionale di Geofisica 537, 9-44.

DOST, B. (1990): Upper mantle structure under Western Europe from fundamental and higher mode surface waves using the NARS array, *Geophys. J. Int.*, **100**, 131-151.

DREGER, D.S. and D. HELMBERGER (1990): Broadband modelling of local earthquakes, *Bull. Seism. Soc. Am.*, **80**, 1162-1179.

DUFUMIER, H. and M. CARA (1994): On the limits of linear moment tensor inversion of surface wave spectra, *Pure App. Geophys.*, in press.

DZIEWONSKI, A.M., S. BLOCH and M. LANDISMANN (1969): A technique for the analysis of transient seismic signals, *Bull. Seism. Soc. Am.*, **59**, 427-444.

DZIEWONSKI, A.M. and A.L. HALES (1972): Numerical analysis of dispersed seimic waves, *Methods in Computational Physics*, **11**, ed. B. Bolt, Academic Press, 39-85.

DZIEWONSKI, A.M. and D.L. ANDERSON (1981): Preliminary Reference Earth

Model (PREM), *Phys. Earth Planet. Inter.*, **25**, 297-356.

DZIEWONSKI, A.M., T.A. CHOU and J. H. WOODHOUSE (1981): Determination of earthquake source parameters from waveform data for studies of global and regional seismicity, *J. Geophys. Res.*, **86**, 2825-2852.

DZIEWONSKI, A.M., G. EKSTRÖM, J.H. WOODHOUSE and G. ZWART (1991): Centroid-moment tensor solutions for April-June 1990, *Phys. Earth Planet. Inter.*, **66**, 133-143.

EKSTRÖM, G., A.M. DZIEWONSKI and J.M. STEIM (1986): Single station CMT: application to the Michoacan, Mexico, earthquake of september 19, 1985, *Geophys. Res. Lett.*, **13**, 173-176.

FOULGER, G. R., and B. R. JULIAN (1993): Non-double-couple earthquakes at the Hengill-Greensdalur volcanic complex, Iceland: are they artifacts of crustal heterogeneity ?, *Bull. Seismol. Soc. Amer.*, **38**, 38-52.

FROHLICH, C. (1990): Note concerning non-double-couple source components from slip along surfaces of revolution, *J. Geophys. Res.*, , 6861-6866, 1990

FROHLICH, C., M. RIEDESEL and K. D. APPERSON (1989): Note concerning possible mechanisms for non-double-couple earthquake sources, *Geophys. Res. Lett.*, **16**, 523-526.

FUCHS, K. and G. MULLER (1971): Computation of synthetic seismograms with the reflectivity method and comparison with observations, *Geophys. J. R. Astron. Soc.*, **23**, 417-433.

FUKUSHINA, T., D. SUETSUGU, I. NAKANISHI and I. YAMADA (1989): Inversion for near earthquakes using long-period digital seismograms, *J. Phys. Earth*, **37**, 1-29.

GIARDINI, D. (1983): Regional deviation of earthquakes source mechanisms from the 'double-couple' model, in *Earthquakes: Observation, Theory and Interpretation*, H. Kanamori and E. Boschi eds., North Holland, Amsterdam, 345-352.

GIARDINI, D. (1984): Systematic analysis of deep seismicity: 200 Centroid-Moment Tensor solutions for earthquakes between 1977 and 1980, *Geophys. J. R. astr. Soc.*, **77**, 883-914.

GIARDINI, D. (1992): Moment tensor inversion from MedNet data: (1) large worldwide earthquakes of 1990, *Geophys. Res. Lett.*, **19**, 713-716.

GIARDINI, D. (1993): Teleseismic observation of the November 23, 1980 Irpinia earthquake, *Ann. Geofisica*, **36-1**, 17-25.

GIARDINI, D., E. BOSCHI and B. PALOMBO (1993a): Moment tensor inversion from MedNet data: (2) earthquakes of the Mediterranean, *Geophys. Res. Lett.*, **20**, 273-276.

GIARDINI, D., B. PALOMBO and E. BOSCHI (1993b): The determination of earthquake size and source geometry in the Mediterranean Sea, in *Recent evolution and seismicity of the Mediterranean area*, E. Boschi et al. eds., Kluwer, pp.213-238.

GIARDINI, D., B. PALOMBO and N. A. PINO (1994a): Long-period modelling of MedNet waveforms for the December 13, 1990 Eastern Sicily earthquake, *Ann. Geofisica*, in press.

GIARDINI, D., L. MALAGNINI, B. PALOMBO and E. BOSCHI (1994b): Broad-band moment tensor inversion from single station, regional surface waves for the 1990, NW-Iran earthquake sequence, *Ann. Geofisica*, in press.

GILBERT, F. and G.E. BACKUS (1966): Propagator matrices in elastic wave and vibration problems, *Geophysics*, **31**, 326-332.

HONDA, H. (1934): On the amplitudes of the P and S waves of deep earthquakes, *Geophys. Mag.*, **8**, 153-164.

HEATON, T., TAJIMA, F. and MORI A. W. (1986): *Estimating ground motion using recorded accelerograms, Surveys in Geophysics*, **8**, 25-83.

HERRMANN, R.B. (1973): Some aspects of band-pass filtering of surface waves, *Bull. Seism. Soc. Am.*, **63**, 663-671.

HERRMANN, R.B. (1987): *Computer Programs in Seismology, User's manual Vol. II*, St. Louis University, Missouri.

HERRMANN, R.B., S.K. PARK and C.Y. WANG (1981): The Denver earthquakes of 1967-68, Bull. Seism. Soc. Am., **71**, 731-745.

HOLT, W.E. and T.C. WALLACE (1987): A procedure for the joint inversion of regional and teleseismic long-period body waves, *Geophys. Res. Lett.*, **14**, 903-906.

HUDSON, J.A. (1969): A quantitative evaluation of seismic signals at teleseismic distances. I - Radiation from a point source, *Geophys. J. R. Astr. Soc.*, **18**, 233-249.

JIMENEZ, E., M. CARA and D. ROULAND (1989): Focal mechanisms of moderate-size earthquakes from the analysis of single-station three component surface wave records, *Bull. Seism. Soc. Am.*, **79**, 955-972.

JULIAN, B. R., and S. SIPKIN (1985): Earthquake processes in the Long Valley Caldera, California, *J. Geophys. Res.*, **90**, 11155-11169.

KANAMORI, H. and J.W. GIVEN (1981): Use of long-period surface waves for rapid determination of earthquakes-source parameters, *Phys. Earth Planet. Int.*, **11**, 312-332.

KAWAKATSU, H. (1991): Insignificant isotropic component in the moment tensor of deep earthquakes, *Nature*, **351**, 50-53.

KENNETT, B.L.N. (1983): Seismic wave propagation in stratified media, *Cambridge University Press, Cambridge*.

KIKUCHI, M., and H. KANAMORI (1994): The mechanism of the deep Bolivia earthquake of June 9, 1994, *Geophys. Res. Lett.*, **21**, 2341-2344.

KNOPOFF, L., and M. J. RANDALL (1970): The compensated linear-vector dipole: a possible mechanism for deep earthquakes, *J. Geophys. Res.*, **75**, 4957-4963.

KUGE, K. and H. KAWAKATSU (1990): Analysis of deep non-double-couple earthquake using very broadband data, *Geophys. Res. Lett.*, **17**, 227-230.

KUGE, K. and H. KAWAKATSU (1992): Deep and of intermediate-depth non-double-couple earthquakes: interpretation of moment tensor inversions using various passbands of very broadband data, *Geophys. J. Int.*, **111**, 589-606.

KUGE, K. and H. KAWAKATSU (1993): Significance of non-double-couple componente of deep and intermediate earthquakes: implications from moment tensor inversion of long-period seismic waves, *Phys. Earth plant. Int.*, **75**, 243-266.

KULHANEK, O. (1990): *Anatomy of seismograms*, Elsevier Science Publishers B.V.

MILLS, J.M. and T.J. FITCH (1977): Thrust faulting and crust-mantle structure of East Australia, *J. Geophys. Res.*, **48**, 351-384.

MAZZA, S. and A. MORELLI (1992): Background seismic noise from MedNet very-broad band stations, *Proceedings and Activity report 1988-1990*, XXII General Assembly of the European Seismological Commission, **1**, 197-202.

MOINFAR, A.A. and A. NADERZADEH (1990): An immediate and preliminary report on the Manjil, Iran earthquake of 20 June 1990, Building and Housing Research Center, Ministry of Housing and Urban Development, **119**, 68 pp.

NAKANISHI, I. and H. KANAMORI (1982): Effects of lateral heterogenity and source process time on the linear moment tensor inversion of long period Rayleigh waves, *Bull. Seism. Soc. Am.*, **72**, 2063-2080.

NAKANISHI, I., T. MORIYA and M. ENDO (1992): The November 13, 1990 earthquake off the coast of the Primorskij region, the Eastern Russia, *Geophys. Res. Lett.*, **19**, 549-552.

NESTEROF, A.N. and T.B. IANOVSKAIA (1988): Horizontal lithospheric heterogeneity in Southwestern Europe from surface wave observations (in russian), *Rev. Russian Acad. Scien., Earth Scien.*, **11**, 3-16.

PANZA, G., S. MÜLLER and G. CALCAGNILE (1980): The gross features of the litosphere-astenosphere system in Europe from seismic surface waves and body waves, *Pure Appl. Geophys.*, **118**, 1209-1213.

RITSEMA, J. and T. LAY (1993): Rapid source mechanism determination of large ($M_w \geq 5$) earthquakes in the western united states, *Geophys. Res. Lett.*, **20**, 1611-1614.

ROMANOWICZ, B. and G. SUAREZ (1983): On an improved method to obtain the moment tensor and depth of earthquakes from the amplitude spectrum of Rayleigh waves, *Bull. Seismol. Soc. Am.*, **73**, 1513-1526.

ROMANOWICZ, B., D. DREGER, M. PASYANOS and R. UHRHAMMER (1993): Monitoring of strain release in central and northern California using broadband data, *Geophys. Res. Lett.*, **20**, **15**, 1643-1646.

RUSSELL, D.R., R.B. HERRMANN and H.J. WHANG (1988). Application of frequency variable filters to surface-waves amplitude analysis, *Bull. Seism. Soc. Am.*, **78**, 339-354.

SAXTON J.L., A.J. RUDMAN and J. MEAD (1977): Ellipticity of Rayleigh waves in the Midwest, *Bull. Seism. Soc. Am.*, **67**, 369-382.

SIPKIN, S.A. (1986): Estimation of earthquakes source parameter by the inversion of waveform data: global seismicity, 1981-1983, *Bull. Seism. Soc. Am.*, **76**, 1515-1541.

SNIEDER, R. (1988): Large-scale waveform inversion of surface waves for lateral heterogeneity 2. Application to surface waves in Europe and the Mediterranean, *J. Geophys. Res.*, **93**, 12.067-12,080.

STEIM, J. (1986): *A broad-band seismic station*, Ph.D. Thesis, Harvard University.

STIMPSON, I. G., and R. PEARCE (1987): Moment tensors and source processes of three Sea of Okhotsk earthquakes, *Phys. Earth Planet. Inter.*, **47**, 107-124.

TAKEUCHI, H. and M. SAITO (1972): Seismic surface waves, in *Methods of computational Physics*, **11**, Academic Press, New York.

THIO, H.K. and H. KANAMORI (1994): Moment tensor inversions for local earth-

quakes using surface waves recorded at TERRAscope, *Bull. S. Soc. Am.*, in press.

THIO, H.K., K. SATAKE, M. KIKUCHI and H. KANAMORI (1990): On the Sudan, Iran and Philippines earthquakes of 1990 (abstract), *EOS, Trans. AGU*, **71**, 1438.

WIELANDT, E. and G. STRECKEISEN (1982): The leaf-spring seismometer: design and performance, *Bull. Seism. Soc. Am.*, **72**, 2349-2367.

WIELANDT, E. and J.M. STEIM (1986): A digital very-broad-band seismograph, *Annales Geophysicae*, **4B3**, 227-232.

WOODHOUSE, J.H. (1980): Efficient and stable methods for performing seismic calculations in stratified media, in *Physics of the Earth Interior, Proc. Int. School of Physics "E. Fermi"*, **78**, 127-151, North-Holland.

WOODHOUSE, J.H. (1988): The calculation of eigenfrequencies and eigenfunctions of the free oscillations of the Earth and the Sun, in *Seismological Algorithms*, ed. D. J. Doornbos, pp.321-370, Academic Press.

WOODHOUSE, J. H. and DZIEWONSKI, A. D. (1984): Mapping the upper mantle: three dimensional modeling of Earth structure by inversion of seismic waveforms, *J. Geophys. Res.*, **89**, 5953-5986.

ZIELHUIS, A. and G. NOLET (1991): A 3D S velocity model for Europe obtained with partitioned waveform tomography, *EOS, Trans Am. Geoph. Un.*, **72**, 349.

Figure Captions

Table III.1. Earthquake parameters for the large global earthquakes of 1990 analyzed in this study. Magnitudes m_b from NEIC, and seismic moments M_0 obtained here (in $dyne \cdot cm$).

Table III.2. Earthquake parameters for the earthquakes of the Mediterranean area (1990-1992) analyzed here.

Figure I.1. Experimental curves of minimum Earth noise averaged over the vertical (continuous line) and horizontal (dashed line) components of MEDNET stations (in power spectral density units; after *Mazza and Morelli, 1992*). The main noise sources are identified.

Figure I.2. The range of seismic noise and signals from 10000 seconds to 10 Hz. Expected levels of earthquakes over a range of magnitudes at 30 degrees epicentral distance are compared with observed peak signal levels (at VBB station HRV) and several models of minimum ambient noise. Units are peak-to-peak acceleration per 1/6 decade. Broad-band acceleration for the events of September 19, 1985 and December 23, 1985 and a local earthquake are shown as horizontal bars, one octave wide above the 1/6 decade spectrum (from *Steim, 1986*).

Figure I.3. Frequency response of the VBB instrument (a) and of other standard seismographs: a broad-band STS (b), a WWSSN (c), a long period SRO (d), a short period SRO (e). The horizontal scale spans frequencies between 1 mHz and 10 Hz; vertical scale is in dB measured from the plateau of the VBB response.

Figure I.4. Technical scheme of a VBB station of the MEDNET network. The core of the station is the station processor, based on the 68000 Motorola architecture. Power supply (UPS) can be provided either by electric power or by solar panels. Output signal is recorded on site on 150 Mbytes streamer-tape or on a DAT, and it is buffered on a 40 Mbytes disk for telemetered access, performed via phone link.

Figure I.5. (A) Vertical record of the July 16, 1990, Luzon earthquake at the MDT MEDNET station. (B) Enlargement (×10) of the early part of the body waves shown in frame A. (C) Enlargement (×100) of the P wave seen in frame B. (D) Enlargement (×1000) of the noise preceding the event.

Figure I.6. Summary of focal mechanisms of the November 23, 1980 Irpinia earthquake obtained from teleseismic observations. For each solution we list the fault plane,

identified by independent evidence, the seismic moment, the publication reference and the data used or method of analysis. Solutions n. 1-3 were obtained by polarity data, n. 4-13 by inversion of long-period data and n. 14 by modelling body waves; n.9-10 and n. 14 also used polarities. Solution n. 2 is found in four sources in the literature. (Modified after *Giardini, 1993*).

Figure II.1. A non-double-couple earthquake may occur if there are two simultaneous couble-couple earthquakes with mechanisms of suitable size and orientation. In (a) a CLVD source with orizontal polar P axis is the sum of an ordinary thrust mechanism and a strike-slip mechanism if both have an east-trending P axis and the same scalar moment. In (b) a CLVD source with a vertical polar T axis is the sum of a thrust mechanism with a north-trending P axis, and a strike-slip mechanism with scalar moment half as large and an east-trending P axis. In (c) a CLVD source with horizontal polar T axis is the sum of a normal faulting mechanism with an east trending T axis and a strike-slip mechanism with scalar moment larger by a factor of $2^{1/2}$ and east-west trending nodal planes.

Figure II.2. Models of non-double-couple sources type expected in ridge-transform regions, obtained by summing normal-faulting and strike-slip mechanisms.

Figure II.3. Dispersion curves for fundamental Rayleigh and Love surface waves for typical oceanic and continental paths (modified from *Kulhanek, 1990*).

Figure III.1. World map with the moment tensors of the largest earthquakes of 1990, listed in Table III.1. For each event we show the best double-couple representation.

Figure III.2. Comparison of fault-planes solutions and moment tensors obtained with different methods for the 1990 earthquakes: the MEDNET solutions obtained here, the CMTs, the moment tensors by USGS and the focal mechanisms by NEIC. For the first three we list the seismic moments in units of $10^{26} dyne \cdot cm$.

Figure III.3. Waveform modelling for station VSL for the deep May 12, Sakhalin event and station MDT for the June 20, Iran event. For each component we show, on the left, six hours of long-period seismograms, low-pass filtered at 100 seconds; data are indicated by continuos lines, synthetic seismograms by dashed lines. On the right are the corresponding frequency spectra for each trace; the signal is tapered at high and low frequencies; the frequency band used in the inversion is indicated (5-7 mHz).

Figure III.4. Geographic distribution of the moment tensors of the 20 Mediterranean earthquakes listed in Table III.2 and of the MEDNET stations operating through 1990-1992 (circled squares mark sites equipped with telemetry). For each event we show the best double-couple representation.

Figure III.5. Comparison of the source geometries obtained here and with the CMT method for the events listed in Table III.2; for all solutions we list the seismic moment in units of $10^{25} dyne \cdot cm$.

Figure III.6. Examples of waveform modelling at regional distance for: (a,b) the large, intermediate depth Romanian earthquake (May 30, 1990), (c,d) a very close station for the May 5, 1990, Potenza event, (e,f) a distant station for the December 13, 1990, Siracusa event, and (g,h) two vertical traces for the small November 11, 1990, Southern Mediterranean earthquake. For each component we show 20 minutes of long-period seismograms, band-passed in the 8-10 mHz frequency bands (data are indicated by continuos lines, synthetic seismograms by dashed lines, displayed only within the time window selected for the inversion).

Figure III.7. Focal mechanisms for the Eastern Sicily, December 13, 1990 earthquake obtained by inverting the joint MedNet data (MedNet) and in single station inversions (AQU, BNI, KEG); for comparison also the CMT mechanism and two fault planes solutions (S1, *Amato et al., 1991*; S2, *De Rubeis et al., 1991*) are also displayed. For all the solutions we list the seismic moment and the variance to the whole MedNet dataset, defined as the ratio between the misfit and the data norm and expressed in percentiles.

Figure III.8. Normalized variance obtained by different moment tensor solutions proportional to the preferred solution for the November 23, 1980, Irpinia earthquake. The seismic moment is estimated to be $M_0 = 2.6 \pm 0.2 \times 10^{19} Nm$.

Figure III.9. (A) Absolute amplitude of the six elements of the moment tensor for five inversions for the Sudan May 20, 1990 earthquake, performed with different minimization contraints (MT1 to MT5); (B) fault mechanisms and inversion parameters for the five solutions in (A) and for a solution obtained including only MEDNET data (MN); we list the constraint ϵ, the seismic moment M_0 (in $dyne \cdot cm$ units), the normalized variance R and the fault plane geometry (strike and slip angles).

Figure III.10. Absolute amplitude of the six elements of the moment tensor for the December 13, 1990 Eastern Sicily earthquake for five inversions performed with different minimization constraints ($\epsilon = 0.0, 0.01, 0.02, 0.05, 1.0$). Upward triangles indicate positive values; downward triangles indicate negative ones. The seismic moments obtained in the five inversions are respectively $4.0, 3.9, 3.9, 3.7, 2.5 \times 10^{24} dyne \cdot cm$; the corresponding normalized variances are 0.043, 0.043, 0.043, 0.045 and 0.125.

Figure III.11. Variance curve obtained in the moment tensor inversion for the deep

May 12,1990 Sakhalin earthquake, perfomed at different trial depths. We display also the moment tensor solutions and the seismic moments (in units of $10^{26} dyne \cdot cm$). On the horizontal scale is the normalized variance, defined as the ratio of the variance over the norm of the data vector.

Figure III.12. Normalized variance, defined as the ratio between the misfit and the data norms, obtained in inversions at different trial depths for the earthquakes of April 21, 1991, Caucasus, December 13, 1990, Eastern Sicily, and June 20, 1990, NW Iran.

Figure III.13. Normalized variance, defined as the ratio between the misfit and the data norms, focal mechanism and seismic moment obtained in inversions at different trial depths for the December 13, 1990 Eastern Sicily earthquake.

Figure III.14. Normalized variance, defined as the ratio between the misfit and the data norms, and seismic moment obtained in moment tensor inversions at different trial depths for the June 20, 1990 Iranian mainshock.

Figure IV.1. The 1990 NW-Iran earthquake sequence. We display the epicentral area, the macroseismic fields of intensity larger than MCS=VI, the surface trace of the earthquake fault break, the mechanisms of the mainshock (90/6/20) and the two aftershocks used in this study (90/6/21, 90/6/24) [modified from *Berberian et al., 1992*].

Figure IV.2. Multiple-frequency forward modelling for the vertical component of station VSL. To the left are the comparisons of data and synthetics computed for the reference model (PREM) in five narrow frequency bands (from top to bottom 8-10, 10-14, 14-18, 18-22, 22-26) and in the whole 8-26 mHz band. The panels in the middle show the corresponding amplitude spectra for data and synthetics (the vertical logarithmic scale spans three orders of amplitude) and the phase difference between the complex spectra of data and synthetics (on a scale of $\pm 4\pi$); to the right are the fit obtained by correcting the path with the smoothed phase difference curve.

Figure IV.3. Dispersion diagram of the vertical component of the VSL recording of the 1990 mainshock, obtained using the MFT algorithm of *Herrmann (1987)*. The left panel contains the dispersion diagram windowed in the 2-5 km/sec group velocity range and 1-30 mHz frequency range. Contours outline the portion of the spectrum with the largest arrivals; squares identify the group velocity of the dominating wave for each frequency. The right panels display the seismograms with time and group velocity. For comparison, the PREM dispersion curve for fundamental Rayleigh waves is shown with a thick line.

Figure IV.4. (A) Group velocity dispersion curves for fundamental Rayleigh waves from PREM (diamonds), for typical oceanic (upper line) and continental (lower line) paths (modified from *Kulhanek, 1990*) and derived for the VSL vertical (upper triangle) and radial (lower triangle) components using the Multiple Filter Technique.
(B) Group velocity dispersion curves for fundamental Love waves from PREM (diamonds), for typical oceanic (upper line) and continental (lower line) paths (*Kulhanek, 1990*) and derived for the VSL transversal component (squares) using the Multiple Filter Technique.
(C) Phase velocity dispersion curves for fundamental Love waves (upper curves) and Rayleigh waves (lower curves) from PREM (diamonds) and those derived for the VSL radial, transversal and vertical components using MFT (squares); the unsmoothed phase delays of the 1990 mainshock are indicated with triangles.

Figure IV.5. Narrow-band and wide-band moment tensor solutions for (A) the June 20, 1990 Iran mainshock, (B) the June 21, 1990 aftershock, and (C) the June 24, 1990 aftershock, and The solutions have been obtained introducing the calibrated phase velocity dispersion curves for Rayleigh and Love fundamental waves (Figure IV.4.). For comparison the CMT solutions are also shown (*Dziewonski et al., 1991*). For each solution we indicate the frequency band used in the inversion (above) and the seismic moment (below), in units of $10^{27} dyne \cdot cm$ for the mainshock and of $10^{24} dyne \cdot cm$ for the two aftershocks. We display the best double-couple focal mechanism for the mainshock (A) and the full moment tensor solutions for the two aftershocks (B).

date	region	lat	lon	d	m_b	M_0
3/3	Fiji	-22.04	175.16	25	6.3	3.2×10^{27}
3/25	Costa Rica	9.89	-84.89	18	6.2	7.8×10^{26}
5/12	Sakhalin	49.04	141.88	590	6.5	7.0×10^{26}
5/20	Sudan	5.32	32.29	15	6.7	5.0×10^{26}
5/30	Romania	45.87	26.67	85	6.7	2.7×10^{26}
6/20	Iran	36.96	49.41	15	6.4	1.1×10^{27}
7/17	Luzon	15.66	121.23	15	6.5	4.5×10^{27}
12/30	N. Britain	-5.09	150.98	200	6.7	1.9×10^{27}

Table III.1.

N	date	region	lat	lon	d	m_b	M_0
1	2/09/90	Algeria	36.75	02.15	12	5.0	1.1×10^{24}
2	5/05/90	S. Italy	40.75	15.85	26	5.3	7.3×10^{24}
3	5/30/90	Romania	45.87	26.67	90	6.7	4.0×10^{26}
4	6/16/90	Albania	39.21	20.54	34	5.5	2.7×10^{24}
5	6/20/90	Iran	36.96	49.41	10	7.7	1.3×10^{27}
6	11/11/90	Med. Sea	33.94	12.04	10	4.7	8.8×10^{23}
7	11/27/90	Yugoslavia	43.87	16.63	10	5.2	2.6×10^{24}
8	12/13/90	Sicily	37.20	15.50	10	5.4	3.7×10^{24}
9	12/21/90	Greece	40.98	22.34	18	5.8	1.7×10^{25}
10	3/19/91	Crete	34.82	26.28	18	5.4	2.0×10^{24}
11	4/10/91	Turkey	37.21	36.01	33	5.1	1.6×10^{24}
12	4/29/91	Caucasus	42.49	43.65	10	6.2	3.7×10^{26}
13	7/12/91	Romania	45.38	21.05	10	5.0	3.2×10^{24}
14	11/21/91	N.Atl.Ridge	48.76	-28.10	10	5.2	1.5×10^{24}
15	12/09/91	Azores	37.21	-24.34	10	5.2	7.3×10^{23}
16	3/13/92	Turkey	40.01	40.01	10	6.7	1.3×10^{26}
17	4/13/92	Holland	51.30	6.30	10	5.4	1.5×10^{24}
18	10/12/92	Egypt	29.90	31.00	10	5.9	9.1×10^{24}
19	10/23/92	Caucasus	42.22	45.12	12	6.7	2.8×10^{25}
20	10/23/92	Morocco	31.30	-4.40	10	5.3	2.9×10^{24}

Table III.2.

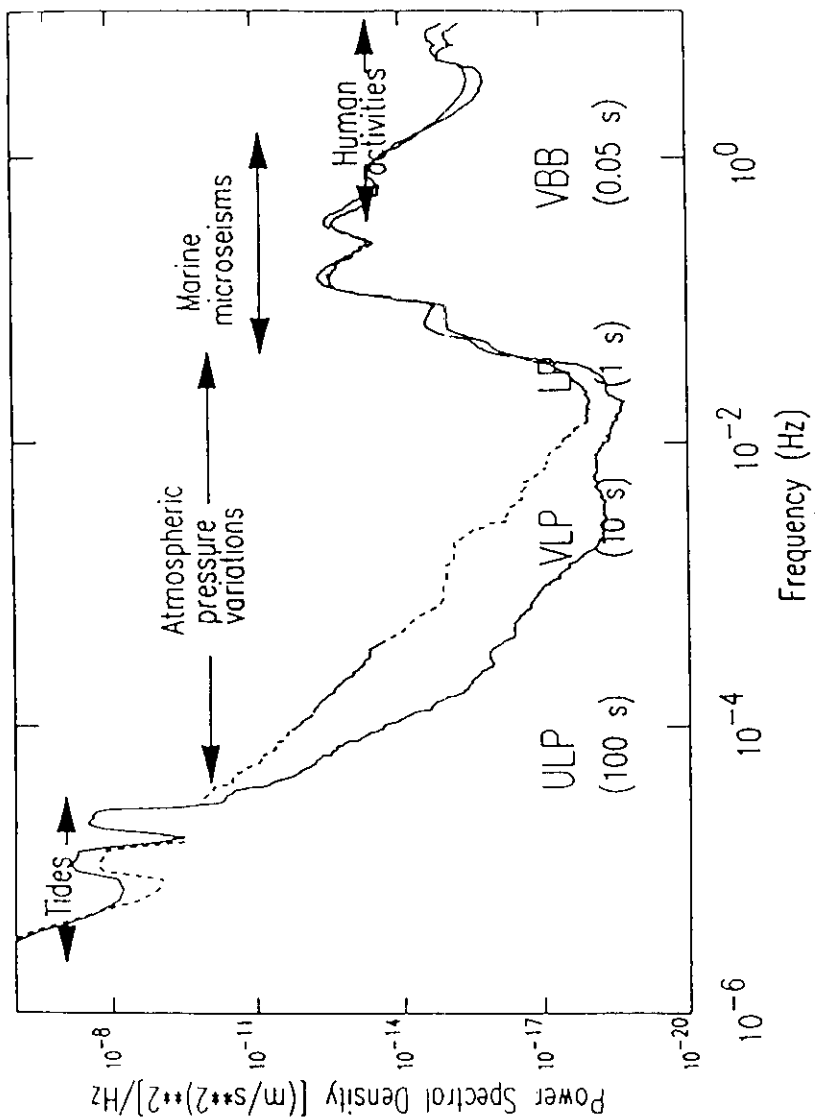

Figure I.1.

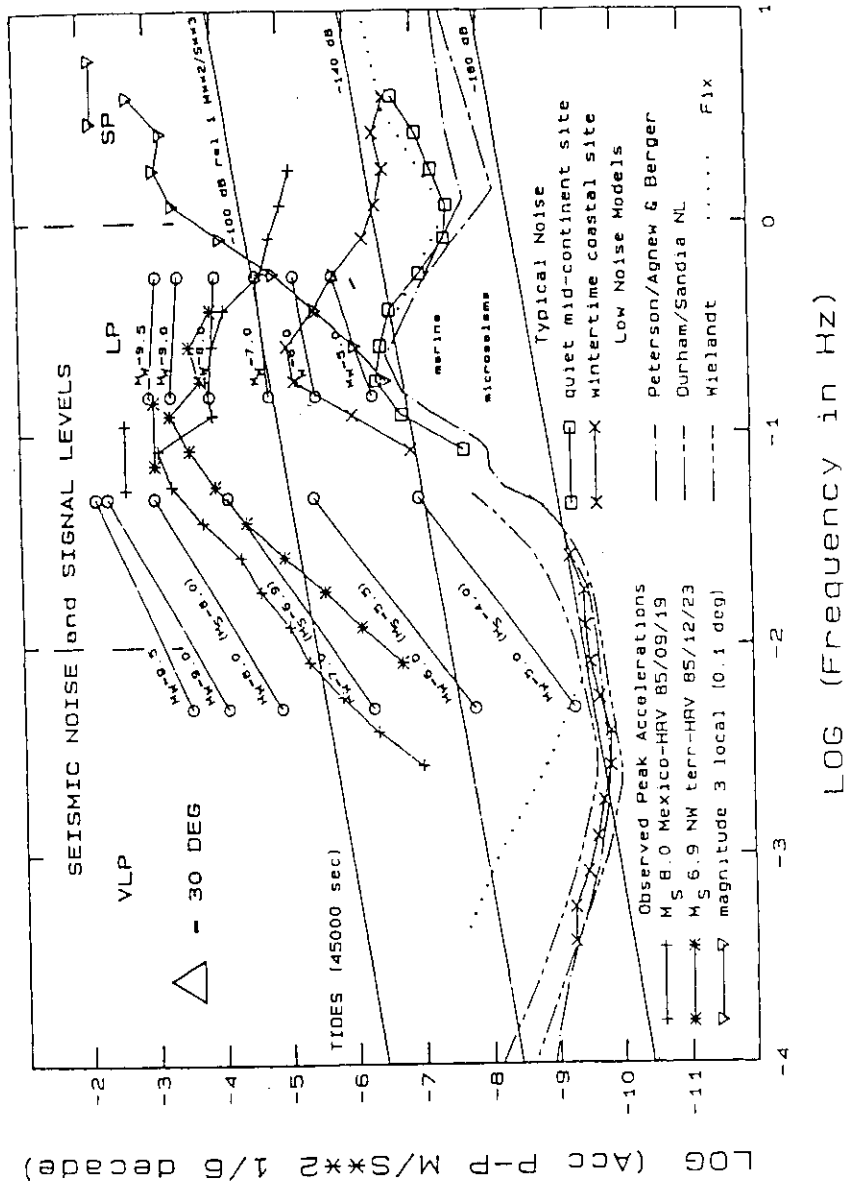

Figure I.2.

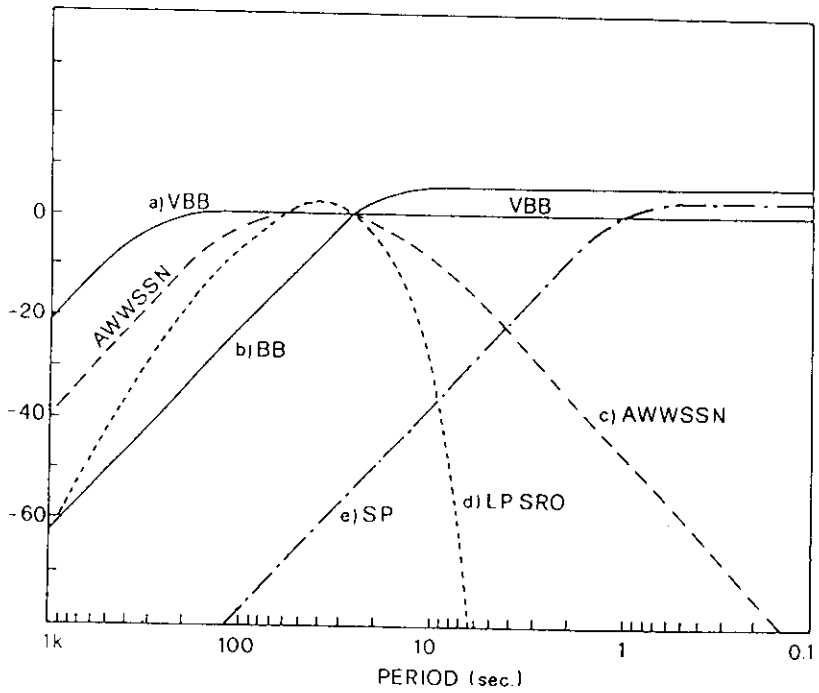

Figure I.3.

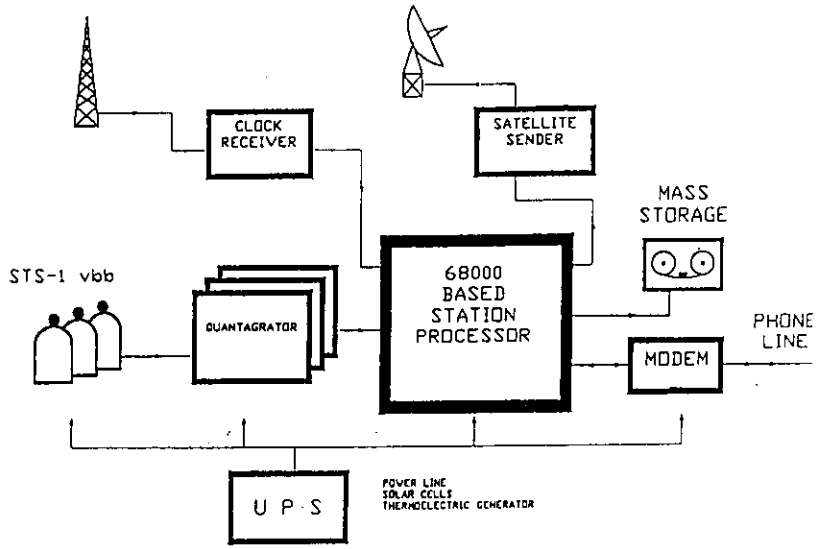

Figure I.4.

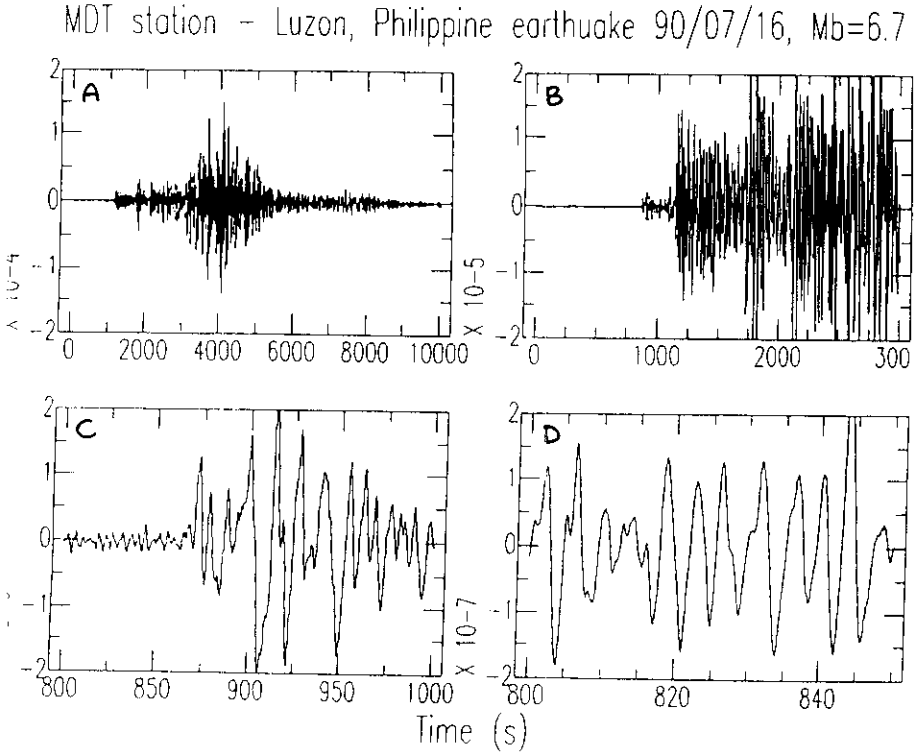

Figure I.5.

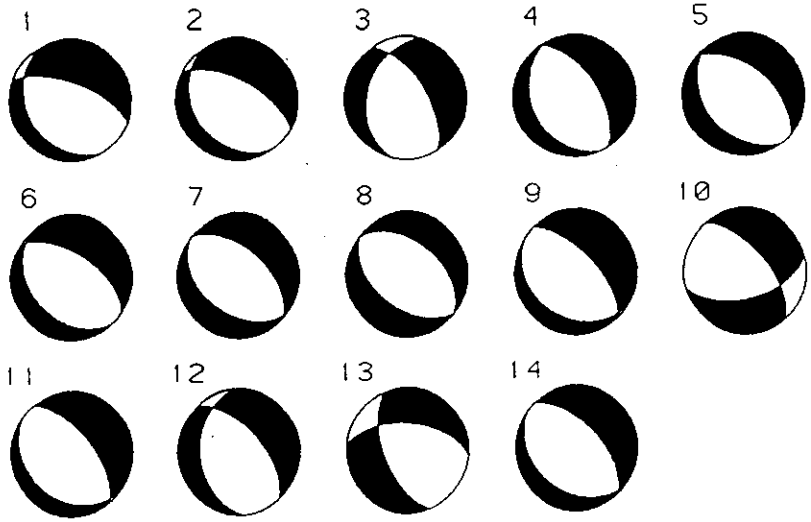

N	Fault *strike*	Plane *dip*	M_0 10^{19} N m	Reference Source	METHOD
1	290°	66°	-	*Gruppo di lavoro Irpinia, 1981*	Polarities
2	298°	64°	-	*Gasparini et al., 1982*	Polarities
"	"	"	-	*Del Pezzo et al., 1983*	Polarities
"	"	"	-	*Martini e Scarpa, 1983*	Polarities
"	"	"	-	*Gasparini et al., 1985*	Polarities
3	328°	62°	-	*this study*	Polarities
4	328°	57°	3.0	*Boschi et al., 1981*	CMT
5	310°	54°	2.4	*Giardini et al.,1984*	CMT
6	305°	58°	2.4	*Ekström et al, 1987*	CMT
7	312°	53°	2.7	*Westaway and Jackson, 1987*	CMT
8	309°	45°	2.8	*Kanamori and Given, 1982*	Surface Waves
9	317°	63°	2.6	*Nakanishi and Kanamori, 1984*	Surface Waves
10	320°	60°	2.0	*Deschamps and King, 1983*	Surface Waves
11	317°	63°	2.6	*this study*	Surface Waves
12	322°	63°	6-10	*Brustle and Müller, 1983*	Love Waves
13	276°	54°	1.3	*Sipkin, 1987*	Body Waves
14	317°	59°	2.1	*Westaway and Jackson, 1987*	Body Waves

Figure I.6.

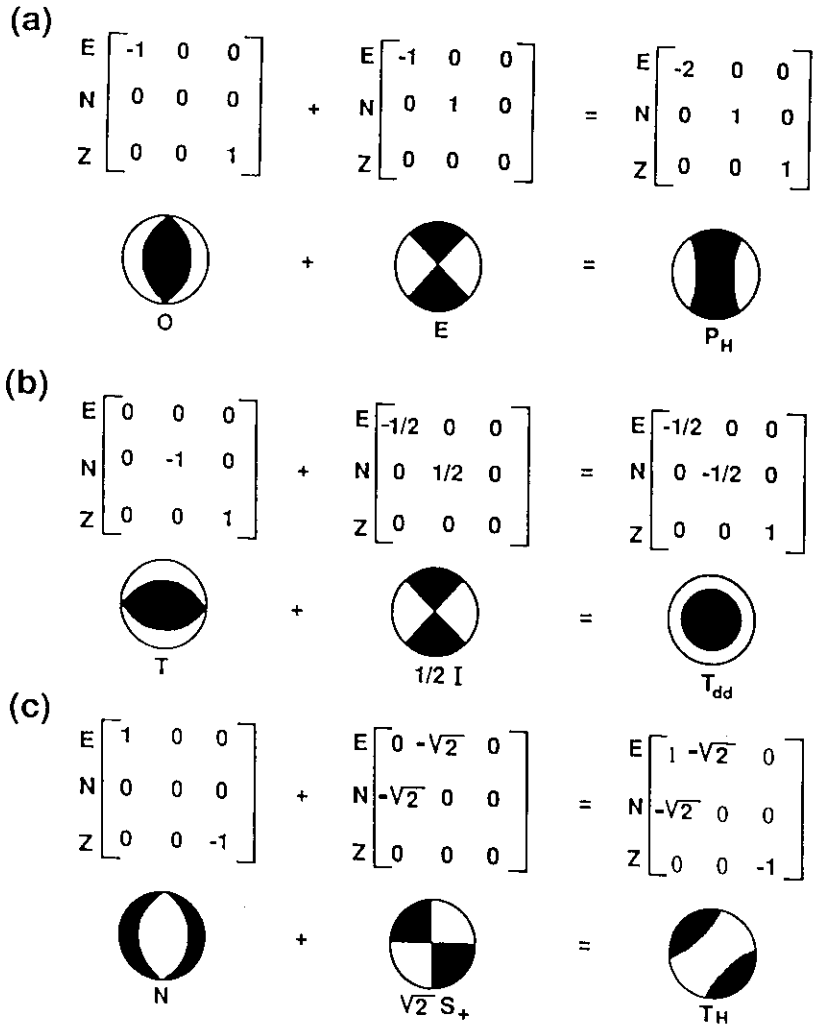

Figure II.1.

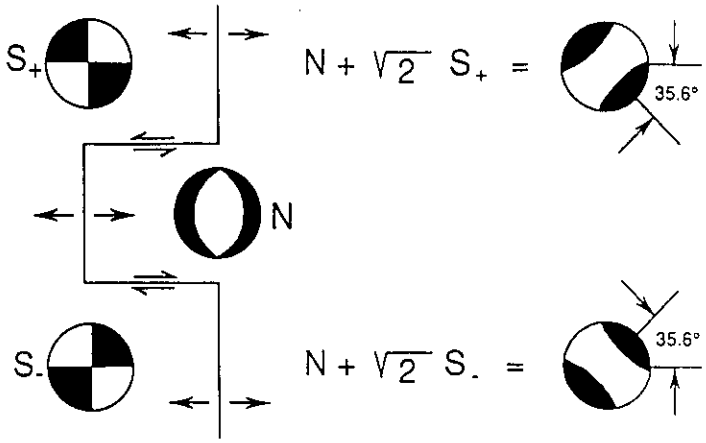

Figure II.2.

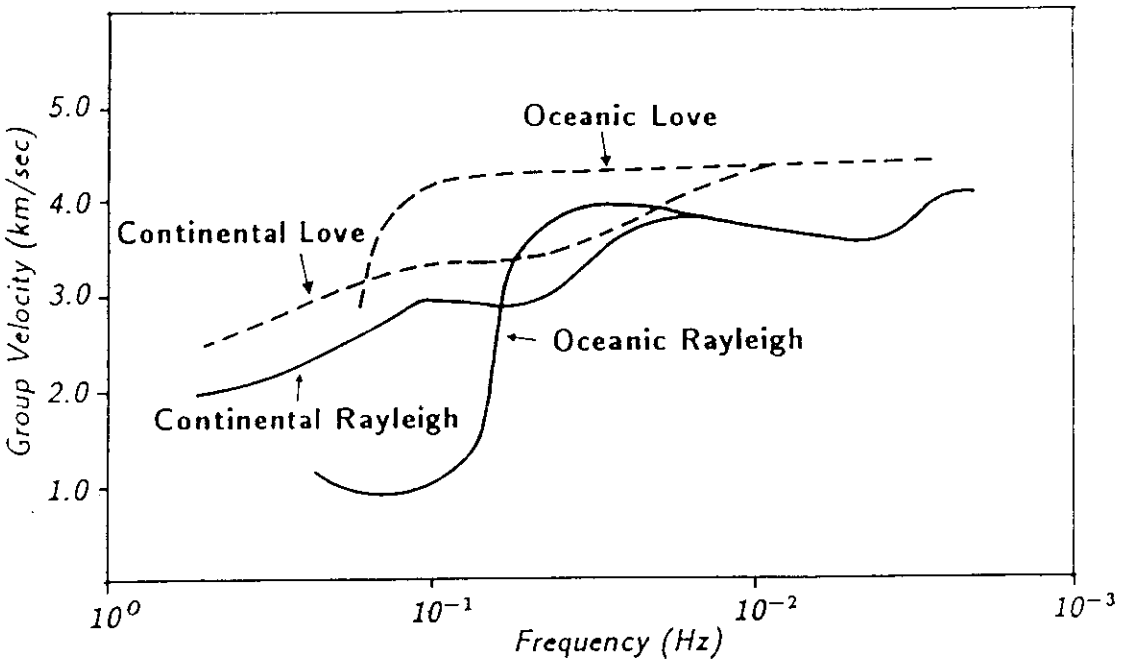

Figure II.3.

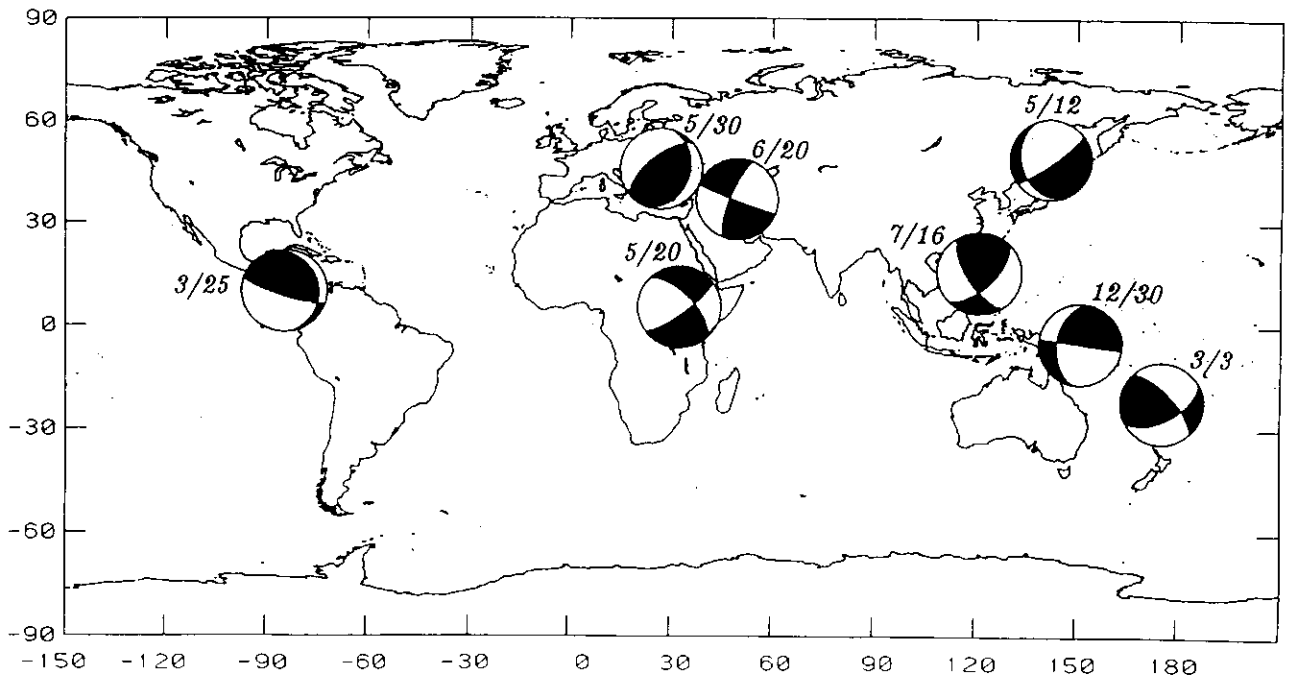

Figure III.1.

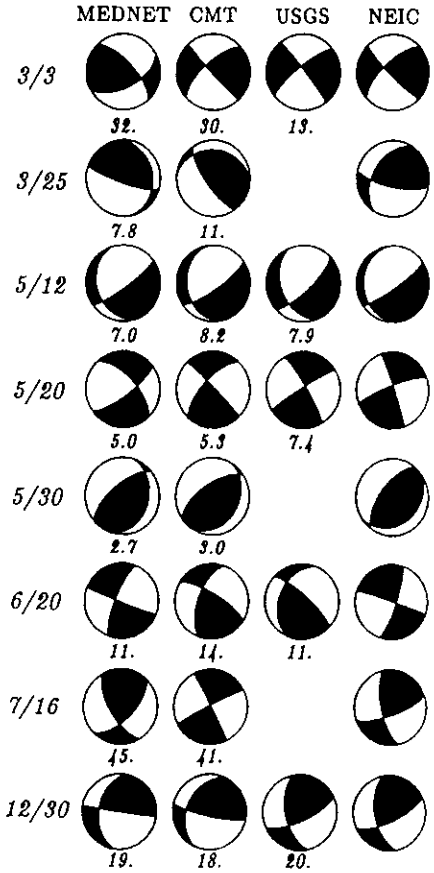

Figure III.2.

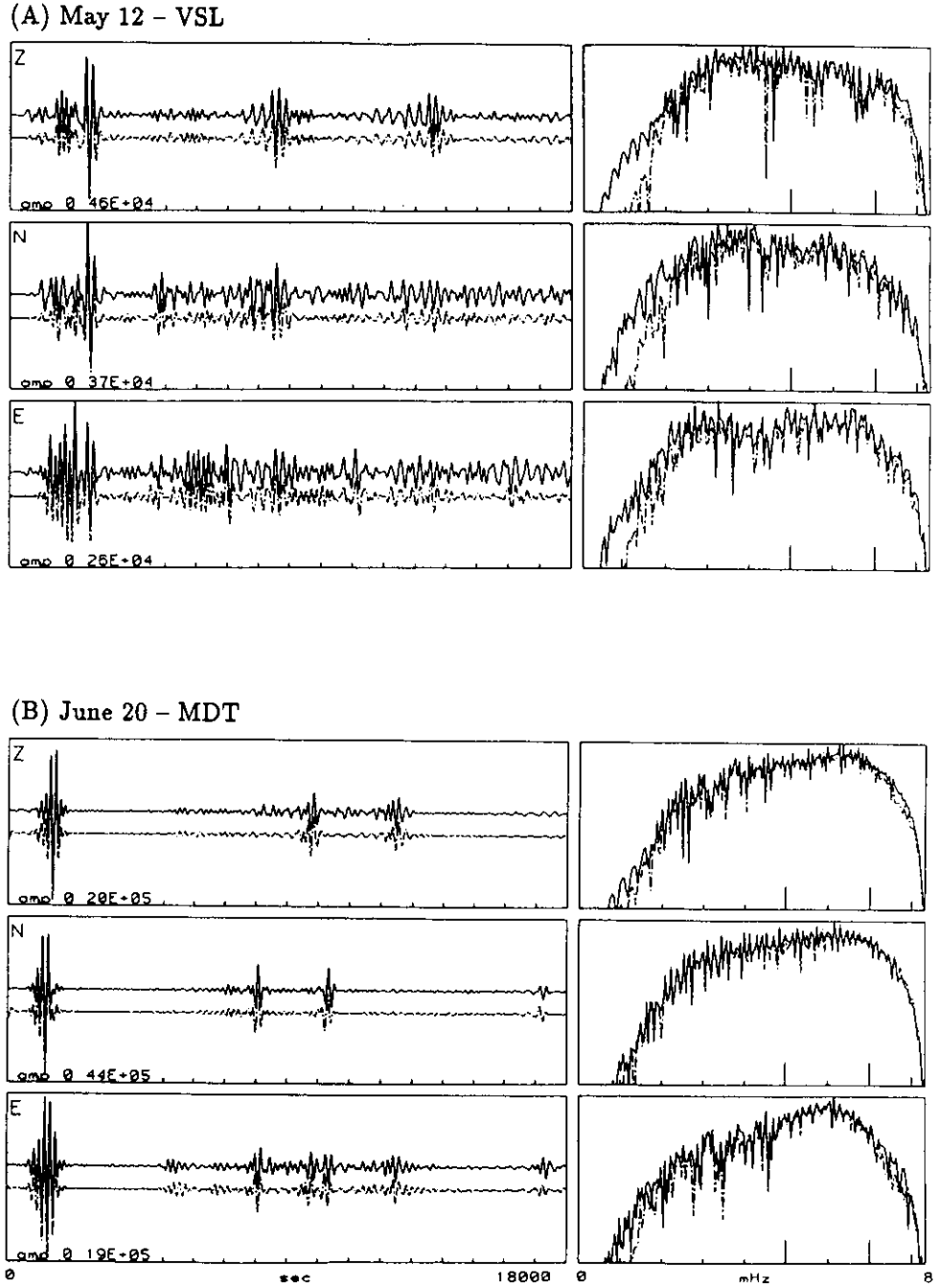

Figure III.3.

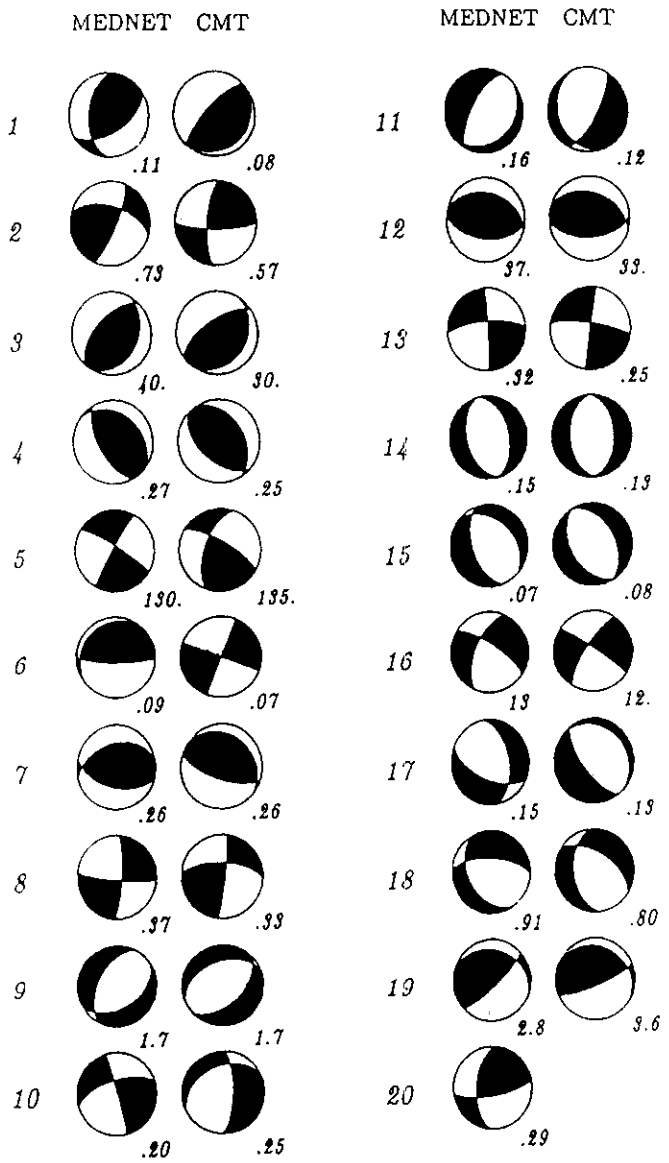

Figure III.5.

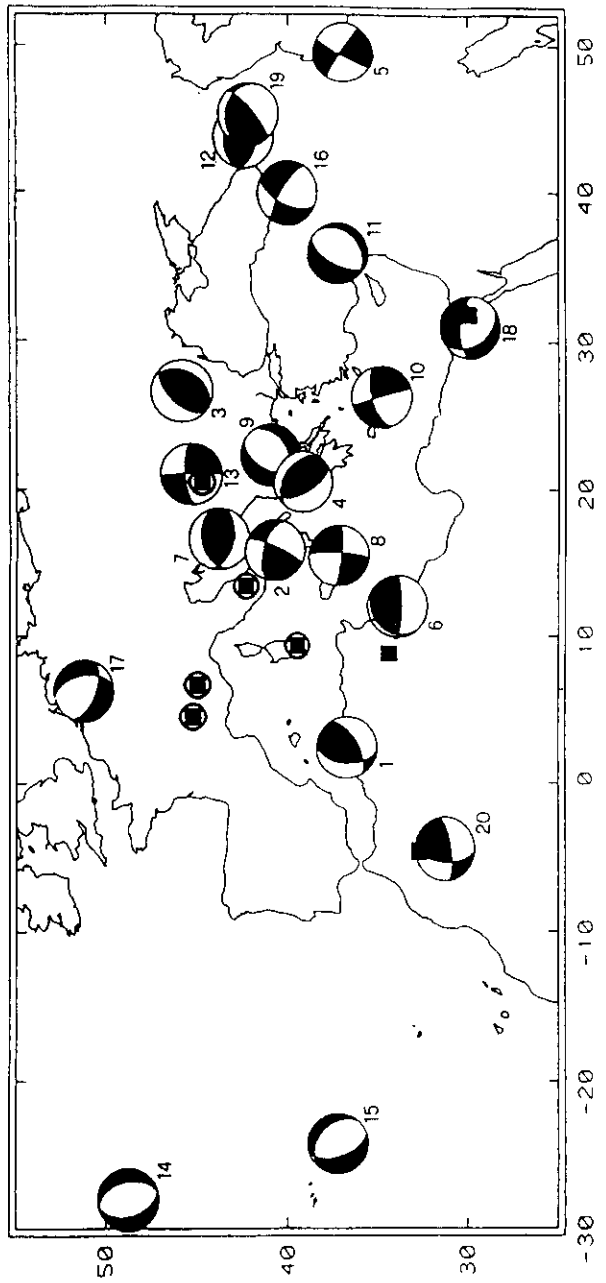

Figure III.4.

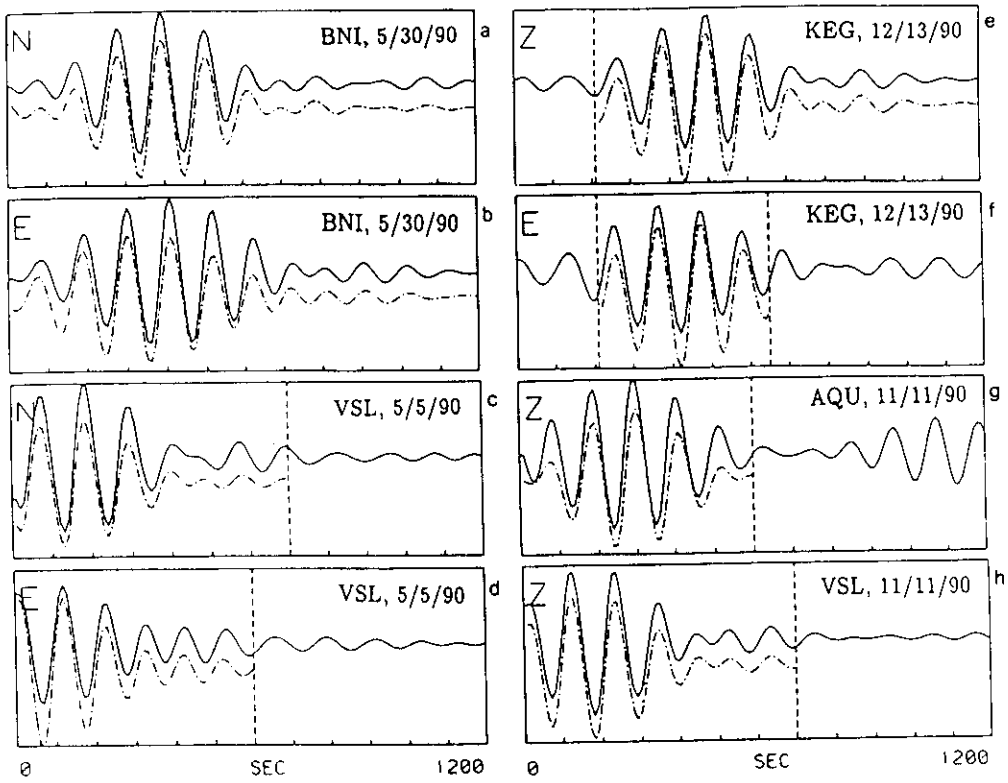

Figure III.6.

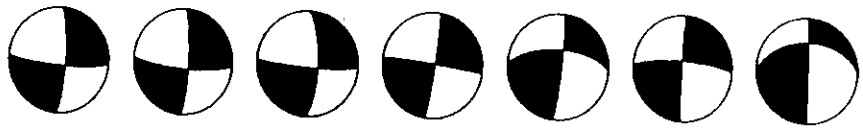

MedNet	AQU	BNI	KEG	CMT	S1	S2
.37/4	.39/4	.23/1	.30/4	.33/18	-/5	-/9

Figure III.7.

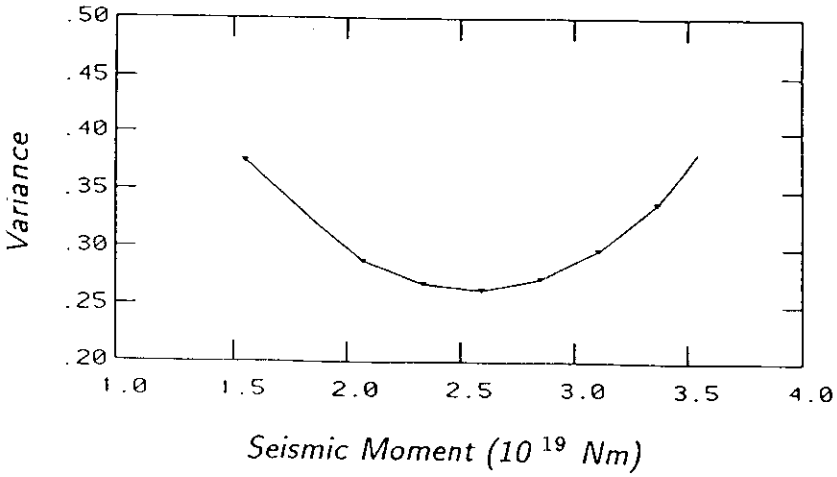

Figure III.8.

5.20.1990 Sudan

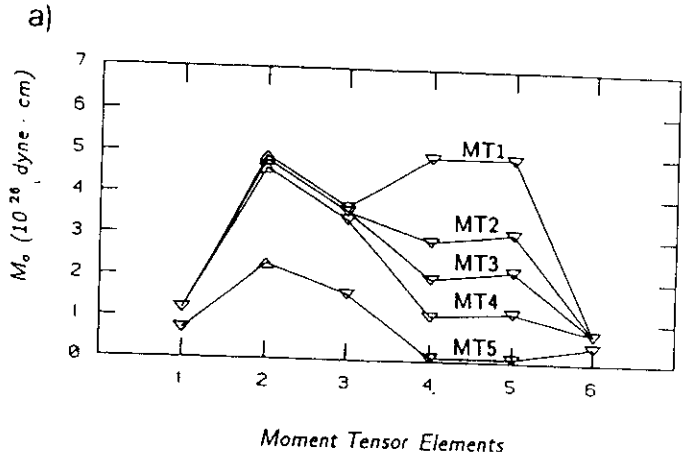

b)

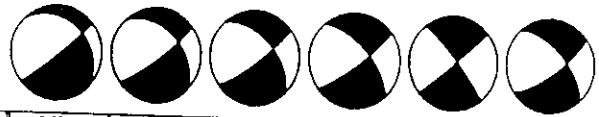

	MT1	MT2	MT3	MT4	MT5	MN
ϵ	.00	.01	.02	.05	1.0	.02
R	.213	.215	.218	.225	.449	.174
M_o	8.2	6.1	5.3	4.5	2.0	5.0
fpl-1	313/32	315/45	316/53	317/65	320/85	316/62
fpl-2	51/85	53/81	53/79	52/79	50/86	55/73

Figure III.9.

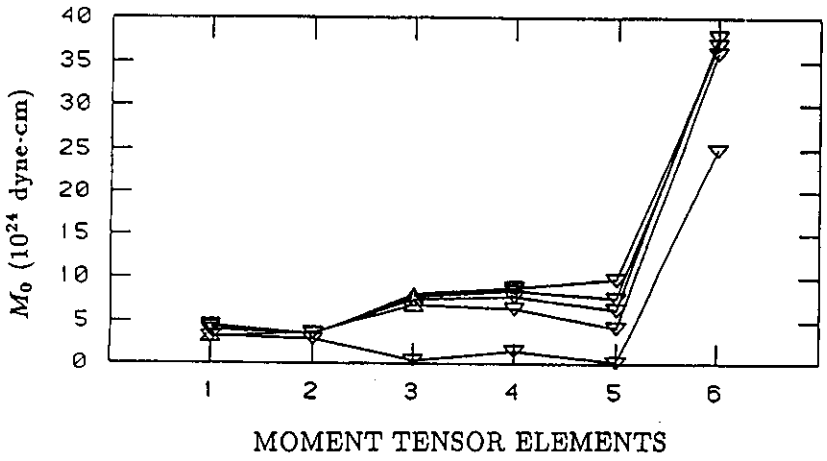

Figure III.10.

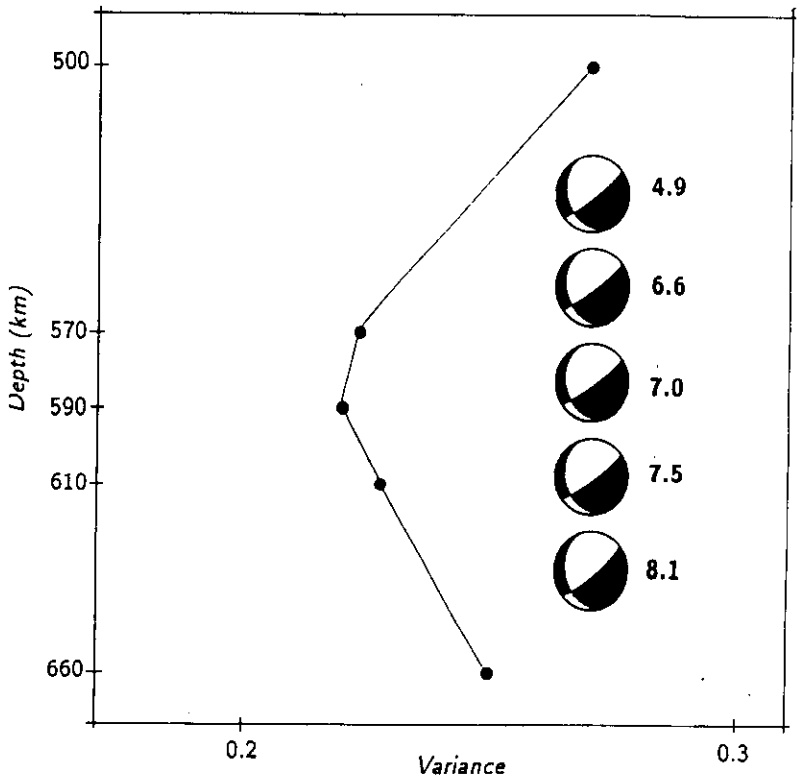

Figure III.11.

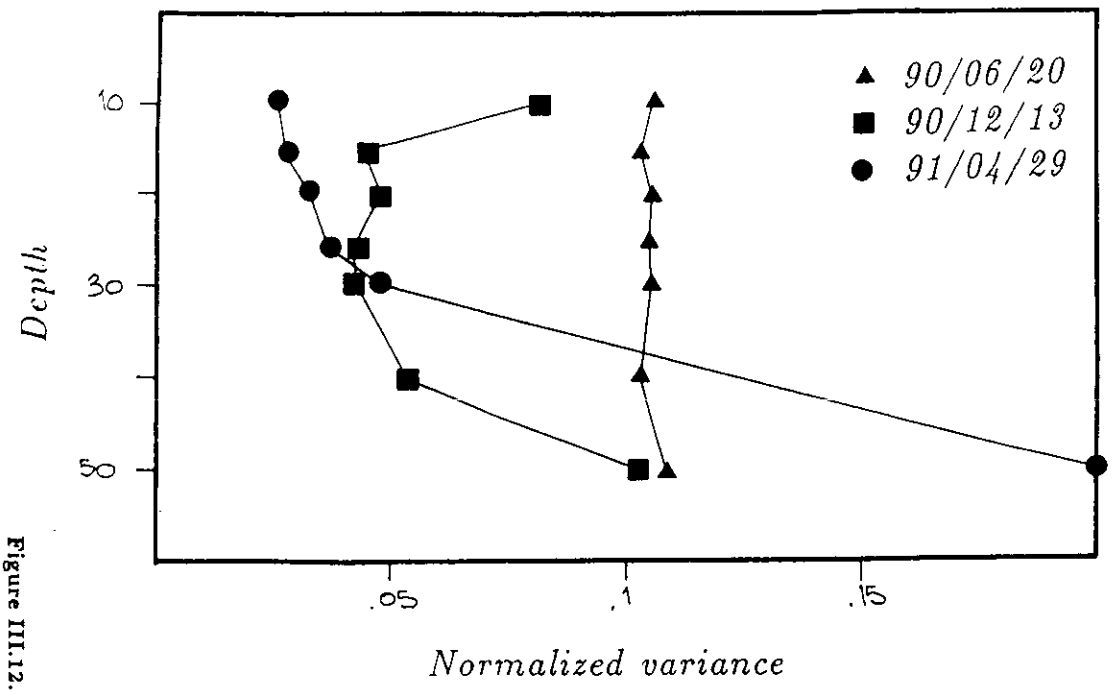

Figure III.12.

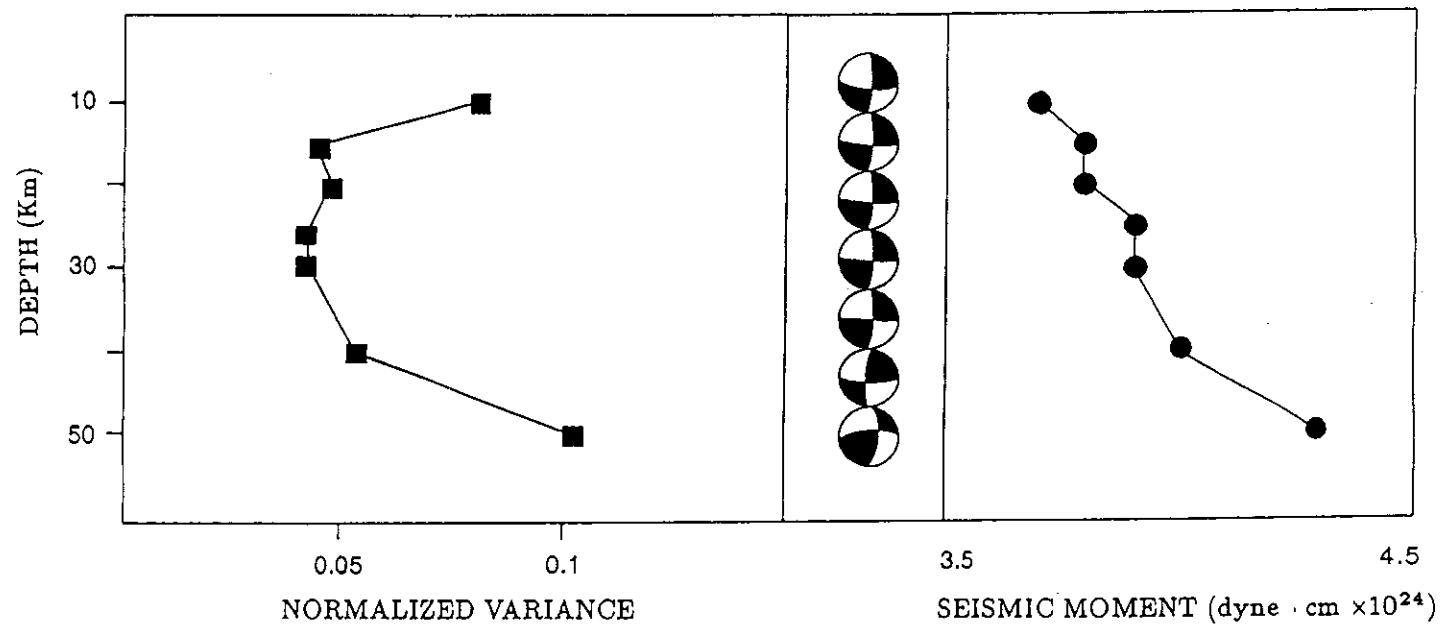

Figure III.13.

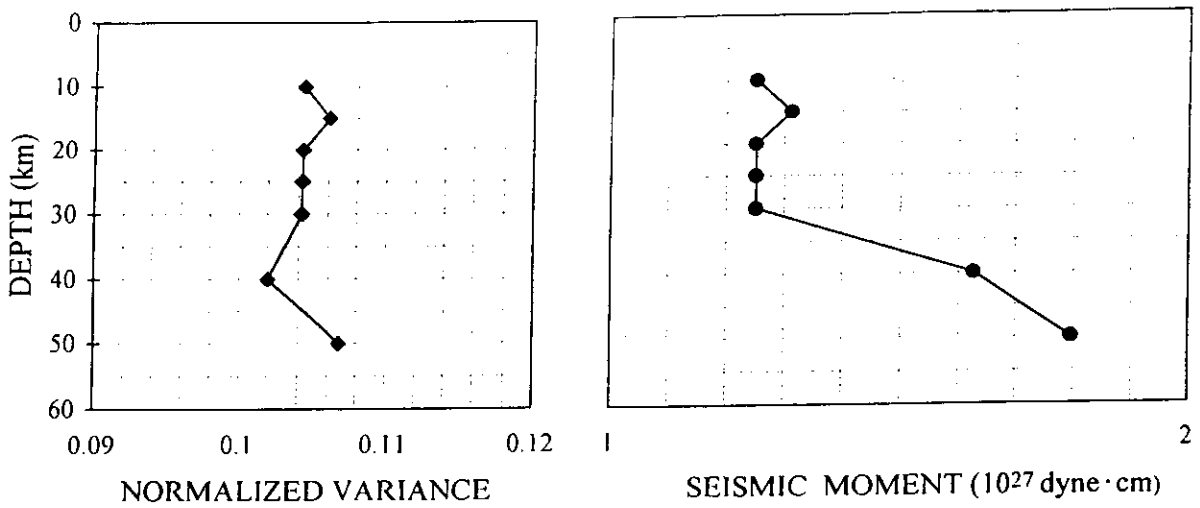

Figure III.14.

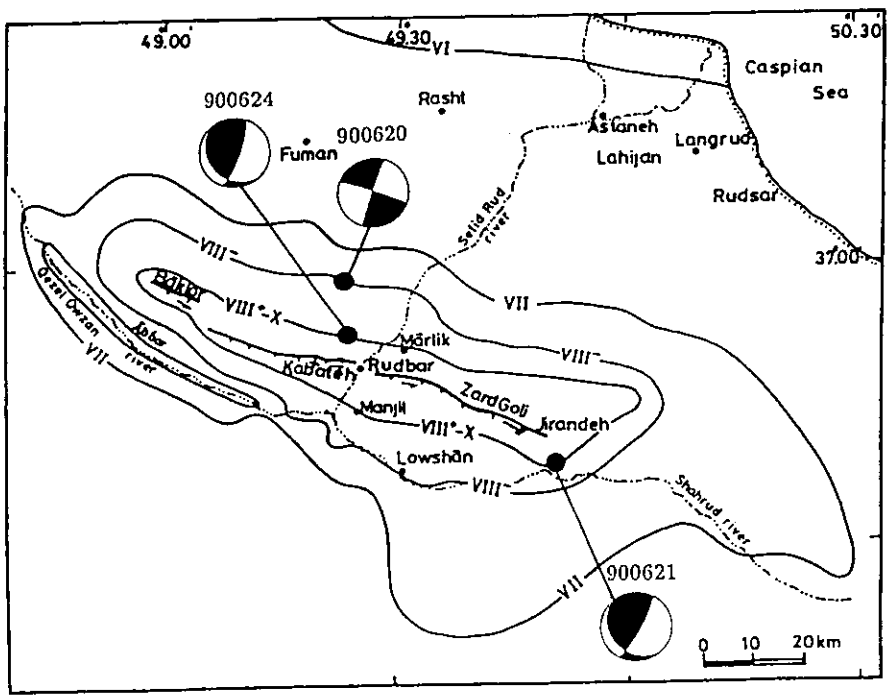

Figure IV.1.

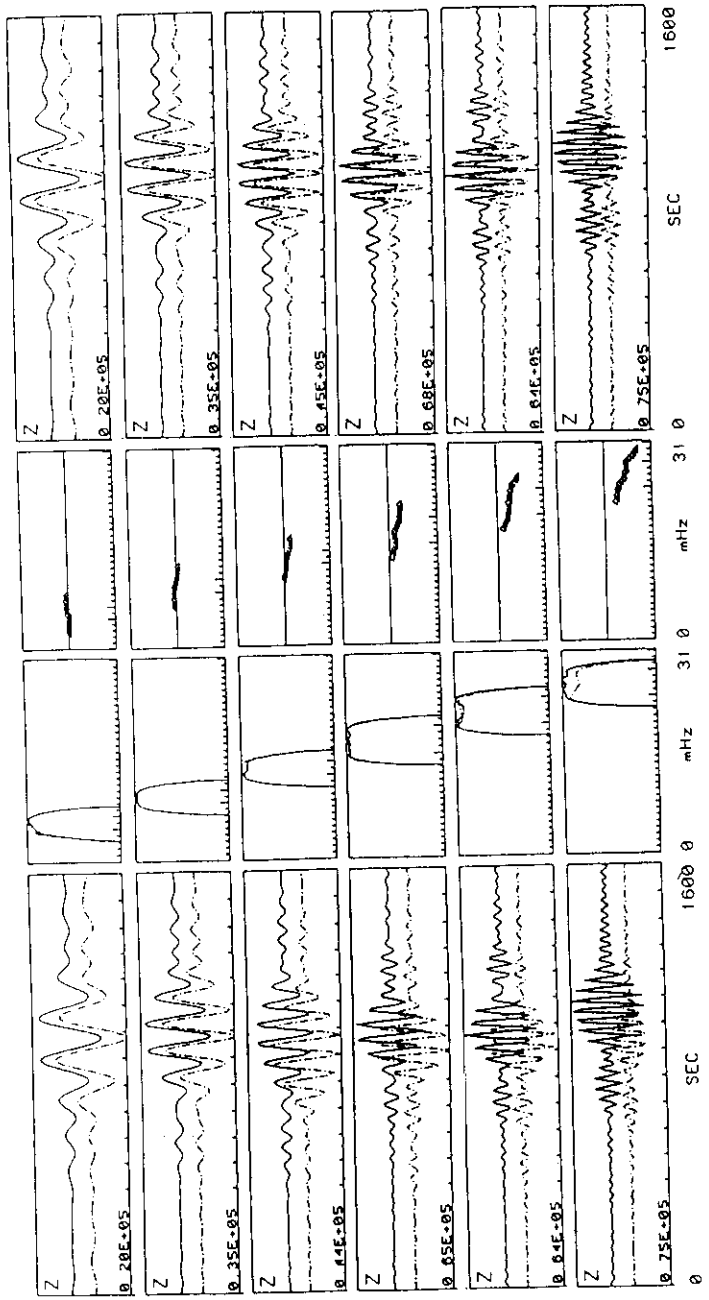

Figure IV.2.

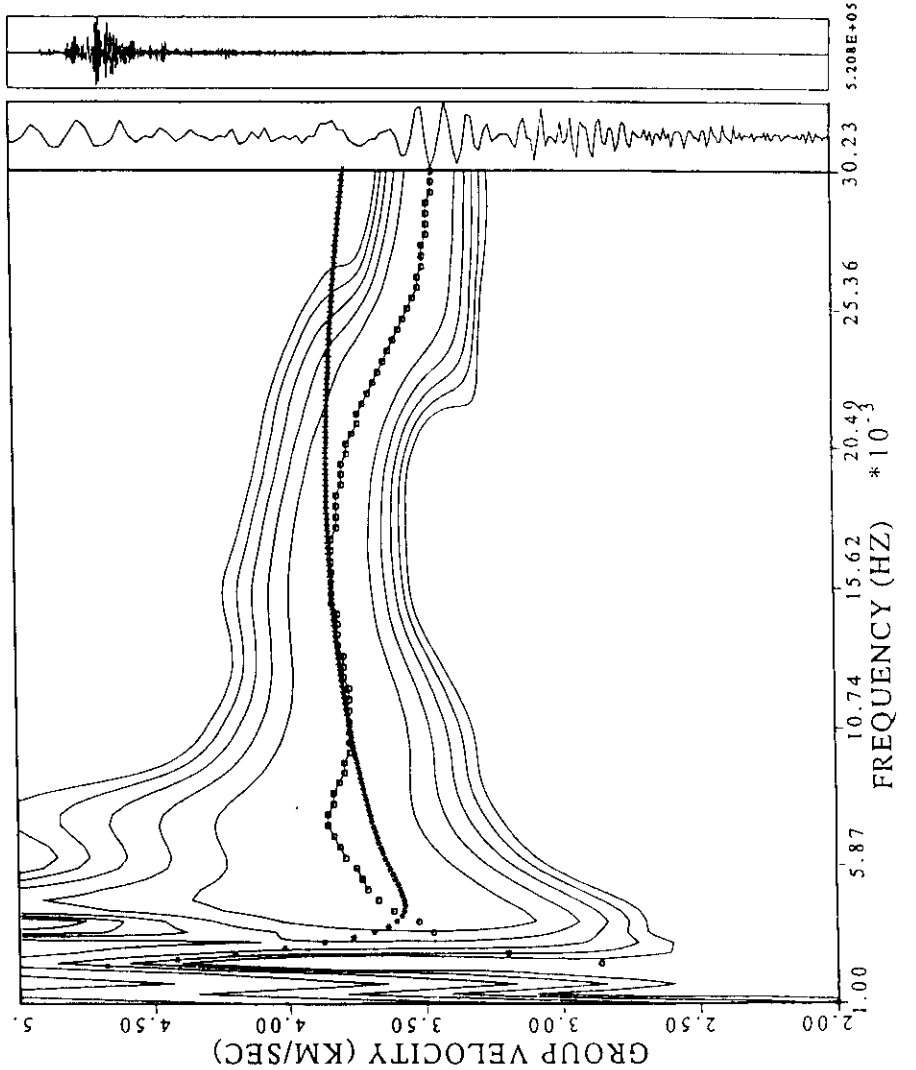

Figure IV.3.

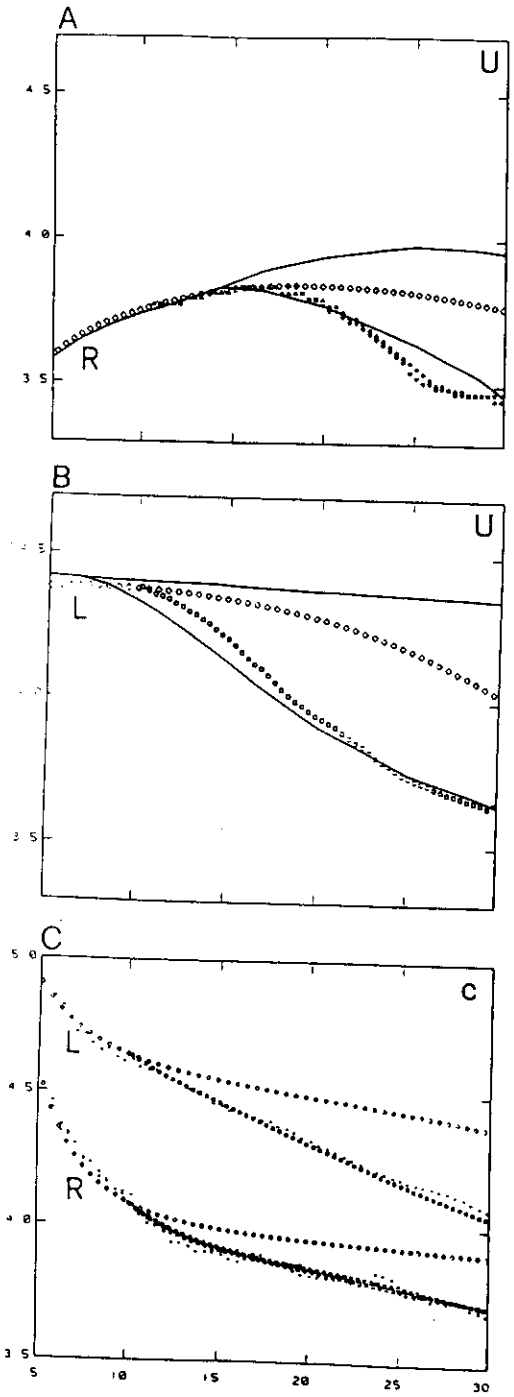

Figure IV.4.

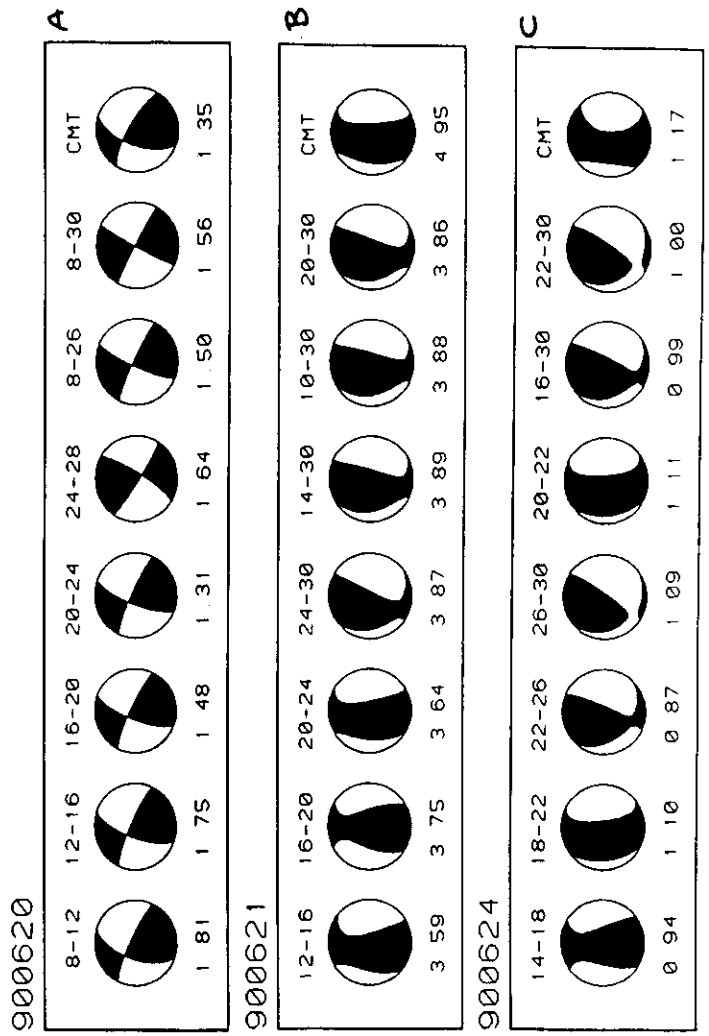

Figure IV.5.